DEVELOPMENT OF PLASMONIC NANOSTRUCTURES AS RAMAN SENSORS FOR THE DETECTION OF ARSENIC ANTIMICROBIALS

by

Jenifier Olavarría-Fullerton

A dissertation submitted in partial fulfillment of the requirements for the degree of

DOCTOR OF PHILOSOPHY
in
Applied Chemistry

UNIVERSITY OF PUERTO RICO
MAYAGUEZ CAMPUS
December 2013

Approved by:

_____	_____
Marco A. De Jesús Ruíz, PhD President, Graduate Committee	Date
_____	_____
Samuel P. Hernández-Rivera, PhD Member Graduate Committee	Date
_____	_____
Félix R. Román, PhD Member Graduate Committee	Date
_____	_____
Marisol Vera, PhD Member Graduate Committee	Date
_____	_____
Robert Ríos, PhD Member Graduate Committee	Date
_____	_____
Ernesto Otero, PhD Representative of Graduate Studies	Date
_____	_____
René S. Vieta, PhD Chairperson, Department of Chemistry	Date

ABSTRACT

Pharmaceutical and Personal Care Products (PPCP's) have been considered as a new category of emerging pollutants due to their persistence in the environment. These compounds have been a cause of concern since they have been detected at trace levels in soils and superficial and underground water. Conventional detection techniques rely on expensive, time consuming procedures and result often result in sample destruction. Surface Enhanced Raman Scattering (SERS) has been considered an attractive tool for the detection and characterization of drugs and bioactive agents since it renders large amounts of structural information which allows unequivocal identification of the analyte. In addition, analysis can be performed with small amounts of sample in aqueous media and signal enhancement allows detection at trace levels. In spite of its advantages, the technique has been limited due to the heterogeneous plasmonic responses provided by traditional substrates.

The work presented herein is focused on the fabrication and development of plasmonic SERS substrates, such as silver/polydimethylsiloxane nanocomposites and hybrid nanostructured arrays, for the study of veterinary drugs in aqueous media. Silver/polydimethylsiloxane (Ag/PDMS) nanocomposites were successfully employed for the detection and characterization of trace amounts of 4-arsanilic acid, roxarsone, and acetarsone in water. The results gathered in this study show that organoarsenic species are distributed into the PDMS surface where the arsonic acid binds onto the embedded silver nanoparticles, enhancing its characteristic 792 cm^{-1} stretching band. The chemisorption of the drugs to the metal facilitates its detection and characterization in the parts per million to parts per billion range. An extensive analysis of the

distinct spectroscopic features of each drug is also presented with emphasis on the interactions of the arsonic acid, amino, and nitro groups with the metal surface.

The combination of electron beam lithography (EBL) and reactive ion etching (RIE) protocols allowed for the construction, testing and validation of nano-arrays with hybrid morphology with multi-wavelength plasmonic response for the detection of arsenic antimicrobials in water. The fabricated substrates consisted of 2500 μm^2 Ag-coated SiO_2/Si pillar nano-arrays of alternating hexagonal and elliptical features. Control of simple fabrication parameters such as inter-particle spacing (gap), and its orientation relative to the laser polarization vector (parallel or orthogonal), result in over a tenfold improvement in the apparent Raman response under optimized conditions. At a 632.8 nm excitation frequency, the best substrate performance was observed on parallel oriented features with a 200 nm gap, with over an order of magnitude increase in the apparent SERS signal relative to standard silver polydimethylsiloxane (Ag/PDMS) nanocomposites. Monitoring of the characteristic As-C stretching band at 594 cm^{-1} allowed the detection of arsenic antimicrobials in water, well within the parts per million range. The surface enhancement factors (SEF) for this substrate at 532, 632 and 785 nm excitation wavelengths were augmented by 5 to 7 orders of magnitude, respectively. The effect of substrate morphology and nanofabrication process on the Raman enhancement factor is presented.

RESUMEN

Los productos farmacéuticos y de cuidado personal (PPCP's) han sido considerados una nueva categoría de contaminantes emergentes debido a su persistencia en el ambiente. Estos compuestos han sido una causa de preocupación ya que han sido detectados a niveles traza en suelos y aguas superficiales y subterráneas. Las técnicas convencionales de detección se basan en procedimientos costosos y de alto consumo de tiempo y en ocasiones resultan en la destrucción de la muestra. La dispersión Raman amplificada por la superficie (SERS) ha sido considerado como una herramienta atractiva para la detección y caracterización de drogas y agentes bioactivos debido a que provee grandes cantidades de información estructural lo que permite la identificación inequívoca del analito. En adición, el análisis puede realizarse con pequeñas cantidades de muestra y la amplificación de señal permite detección a niveles traza. A pesar de sus ventajas, la técnica ha sido limitada debido a las respuestas plasmónicas heterogéneas proveídos por sustratos tradicionales.

El trabajo presentado a continuación está enfocado en la fabricación y desarrollo de sustratos plasmónicos SERS, como nanocompositos de plata/polidimetilsiloxano y arreglos nanoestructurados híbridos, para el estudio de drogas veterinarias en medio acuoso. Los nanocompositos de plata/polidimetilsiloxano (Ag/PDMS) fueron empleados exitosamente para la detección y caracterización de cantidades trazas de ácido 4-arsanílico, roxarsona y acetarsona en agua. Los resultados recopilados en este estudio demuestran que las especies organoarsenicas estan distribuidas en la superficie del PDMS donde el ácido arsónico se enlaza a las nanopartículas de plata incrustados, realzando su banda de estiramiento en 792 cm^{-1}. La chemisorción de las drogas al metal facilita su detección y caracterización en un rango de parte

por millón a parte por billón. Un análisis extensivo de las distintas características espectroscópicas de cada droga es presentado con énfasis en las interacciones del ácido arsónico, amino, y grupos nitro con la superficie metálica.

La combinación de protocolos de litografía por haz de electrones (EBL) y grabado por ion reactivo (RIE) permitieron la construcción, prueba y validación de nanoarreglos de morfología híbrida con respuesta plasmónicos a multiples largos de onda para la detección drogas antimicrobiales de arsénico en agua. Los sustratos fabricados consistieron de nano arreglos 2500 μm^2 de arreglos de pilares de SiO_2/Si cubiertos por plata con características hexagonales y elípticas. Control sobre parámetros simples de fabricación como espacio entre partícula y su orientación relativa al vector de polarización del láser (paralelo u ortogonal), resultan en una mejora de sobre diez veces en la respuesta aparente Raman bajo condiciones optimizadas. A una frecuencia de excitación de 632.8 nm, el mejor rendimiento fue observado para el sustrato con características paralelas con un espacio entre partículas de 200 nm con un aumento de orden de magnitud en la señal aparente SERS relativo a nanocompositos estándares de plata/polidimetilsiloxano (Ag/PDMS). El monitoreo de la banda característica de estiramiento As-C en 594 cm^{-1} permitió la detección de antimicrobiales de arsénico en agua dentro del rango de partes por millón. Los factores de realce por superficie (SEF) calculados para este sustrato empleando longitudes de onda de excitación de 532, 632 y 785 nm fueron aumentados por 5 a 7 órdenes de magnitud, respectivamente. El efecto de la morfología del sustrato y el proceso de nano-fabricación en el factor de realce Raman es presentado.

DEDICATION

To God,
my parents Rodolfo and Kimberly,
my husband William and my daughter Isabella Del Mar

ACKNOWLEDGEMENTS

I would like to express my appreciation and respect to all the people who have, in one way or another lent a hand toward the completion of this work. First, I would like to thank God for giving me the strength, encouragement and patience to reach one of my goals. I would not be where I am today without Him.

I would like to thank my thesis advisor Dr. Marco A. De Jesús for his guidance, patience and support in this work. Thanks for allowing me to be a part of his research group, it has been an honor. I also extend my appreciation to the members of my graduate committee: Dr. Félix Román, Dr. Samuel Hernández, Dr. Marisol Vera and Dr. Robert Ríos for accepting to be part of this work and their collaboration and support in various aspects of the project. I also want to thank all of the professors that have contributed to my professional development with their dedication and effort. Thanks to the University of Puerto Rico, Mayaguez Campus for granting me the opportunity to complete my PhD. Studies.

I would express my gratitude to Dr. Michael J. Sepaniak and the University of Tennessee at Knoxville for granting me the opportunity to form part of his investigation group during my internship practicum. Special thanks to all of the graduate students who collaborated with me during my stay: Sabrina Wells, Deepak Bhandari, Kasey Hill and Lisa Taylor.

I would like to thank Dr. Félix Román and the Center for Education and Training in Agriculture and Related Sciences (CETARS) under grant #2012-01252 and the USDA Grant #2008-02146 for their support during my graduate studies.

A special thanks to the Center for Chemical Sensors and Development (CCSD) directed by Dr. Samuel P. Hernández for granting user access to the Raman instrumentation and facilities.

A special thanks to the entire group members, especially Leonardo, William, Eduardo, John, Pedro, José, Amira, Hilsamar and Oliva, for your unconditional support.

I also want to thank my lab partners: Hector, Raymond, Elena, Grecia, Lina and Queziel. Thanks for your friendship and all the fun times that made this process a more enjoyable one. I wish you all the best and if there is ever anything I can help with just let me know! A special thanks to all my girls who have collaborated with me during the past years in this project: Karla, Legna, Enid and Elena. You were the best and I wish you all success in your future careers.

I would like to thank my friends: Leo, Hector, Hilsamar, Eduardo, John, José, Elena, Grecia, Raymond, Amira, Oliva for your friendship and support. A special mention to the staff of the chemistry department, for their help especially Francheska, Franklyn, Jessica, Lissette, Sindia, Aracelis, Edgard, Enrique, Ayadis and Fernando.

I would like to acknowledge the Center for Nanophase Materials Sciences, which is sponsored at Oak Ridge National Laboratory by the Scientific User Facilities Division, Office of Basic Energy Sciences, U.S. Department of Energy. This research was also supported in part by the following: (1) UPRM Bio Science and Engineering Initiative (BioSEI) under grant #390606; (2) Alfred P. Sloan Foundation; (3) US Environmental Protection Agency STAR program under grant EPA-83274001 with the University of Tennessee; and (4) the Department of Chemistry and Faculty of Arts and Sciences of the University of Puerto Rico, Mayaguez Campus.

I want to give a very special thank you to my parents, Rodolfo, Kimberly, my brothers, R.J. and Kevin, and Jenny for all their love, support and encouragement during all these years. Mom and dad, thanks for always being there when I needed a hand or just someone to listen. Thanks for believing in me. I couldn't have done it without you, I finally made it! To my brothers, thanks for all the fun times! To Jenny, thanks for your support and fun times!

Finally, I want to thank my loving husband, William and beautiful daughter, Isabella Del Mar, for their love, comprehension and patience during this phase of our lives. William, thanks for always believing in me, being there when I needed you the most and for all your support during good times and not so good times. To my little angel, Isa, thanks for filling my days with so much joy, fun and making each and every day worth fighting for.

TABLE OF CONTENTS

LIST OF TABLES

LIST OF FIGURES

LIST OF ABBREVIATIONS

PPCP's	pharmaceuticals and personal care products
U.S. FDA	United States Food and Drug Administration
LC-MS	liquid chromatography with mass spectrometry
ICP-MS	inductively coupled plasma with mass spectrometry
CE-MS	capillary electrophoresis with mass spectrometry
IC-ICP-MS	ion chromatography with inductively coupled plasma with mass spectrometry
SERS	surface enhanced Raman scattering
PDMS	polydimethylsiloxane
Ag	silver
NSL	nanosphere lithography
NIL	nanoimprint lithography
EBL	electron beam lithography
SMSERS	single molecule surface enhanced Raman scattering
Ag/PDMS	silver/polydimethylsiloxane
PVD	physical vapor deposition
HOMO	highest occupied molecular orbital
LUMO	lowest occupied molecular orbital
RIE	reactive ion etching
EPL	electron beam projection lithography
SEM	scanning electron microscope
nTP	nanotransfer printing

LSPs	localized surface plasmons
FDTD	finite differential-time domain
FEM	finite-elements methods
EM	electromagnetic
DDA	discrete dipole approximation
MMP	multiple multipole method
USDA	United States Department of Agriculture
LSPR	localized surface plasmon resonance
Au/PDMS	gold/polydimethylsiloxane
He-Ne	helium-neon
L	length
W	width
H	height
PEH	parallel ellipse hexagon
OEH	orthogonal ellipse hexagon
IPA	isopropyl alcohol
DIW	deionized water
SiO_2	silicon dioxide
Ag/SiO_2	silver/silicon dioxide
4-ABT	4-aminothiophenol
EMF	electromagnetic fields
PML	perfectly-matched layers
CV	coefficient of variation

SEF	surface enhancement factor
a.u.	arbitrary units
ppb	parts per billion
ppt	parts per trillion

LIST OF SYMBOLS

$\hbar\omega_v$	energy of the vibration
E_L	incident photon energy
E_s	scattering photon energy
P	dipole moment
α	polarizability of the molecule
t	time (seconds)
v_0	frequency (Hz)
q	physical displacement
q_0	maximum displacement
ν_m	frequency of the molecule
S_0	electronic-ground-state
S_1	excited state
E	strength of applied field
$\varepsilon_1(w)$	complex, frequency-dependent dielectric function of the metal
ε_2	external dielectric constant
Re	real part
Im	imaginary part
I_{NRS}	intensity of normal Raman scattering
I_{SERS}	intensity of SERS
K(ν)	instruments response factor

N_{NRS}	number of molecules in probe volume in normal Raman scattering
$\frac{\partial \sigma}{\partial \Omega}$	differential cross-section of the molecule
$I_{0,NRS}$	laser intensity of normal Raman scattering
$I_{0,SERS}$	laser intensity of SERS
ν^4	frequency dependence of the scattering process
t_{NRS}	acquisition time for normal Ramanscattering
t_{SERS}	acquisition time for SERS
I_{SERS}	intensity of SERS scattering
I_{vol}	intensity of NRS scattering
N_{SURF}	number of molecules adsorbed on SERS substrate
N_{vol}	number of molecules sampled in bulk
λ	wavelenght
$\|E\|^2$	electromagnetic
cm^{-1}	wavenumber
$\lambda_{532\ nm}$	wavelength at 532 nm
$\lambda_{785\ nm}$	wavelength at 785 nm
Å	Armstrong
α'	planar Raman active modes
α''	non-planar Raman active modes

ν_{as}	asymmetric stretching
ν_{s}	symmetric stretching
ω	wagging
δ	bending

CHAPTER 1

INTRODUCTION TO PRINCIPLES OF RAMAN AND SERS SPECTROSCOPY AND PLASMONIC SUBSTRATES

1.1. Raman Spectroscopy

The low polarizability of water combined with advances in vibrational microscopy and laser technology, have made Raman spectroscopy a promising tool for the analysis of drugs and bioactive agents in aqueous media.[1] Scalability for field operations, low sample requirements, and the large amounts of structural information it provides makes the technique particularly attractive for the analysis of antimicrobial drugs.

Raman spectroscopy is based on a light scattering phenomena that involves the simultaneous adsorption of an incident photon and the emission of another photon called scattered photon.[2]Figure1.1 illustrates the various dispersion events that occur upon the interaction of electromagnetic radiation with chemical substances. Elastic scattering, also known as Rayleigh scattering, is a process where there is no energy transfer between the molecule and the photon, therefore the incident and scattered photon result in no energy loss. In contrast, during inelastic scattering known as Raman scattering the incident and scattered photon have different energy since there is a transition between vibrational/rotational levels in the molecule. This leads to two possible interactions:

Stokes scattering: The molecule is excited from a lower to a higher energy-level; that is from vibrational ground state $\nu = 0$ to the first vibrational excited state $\nu = 1$,

consequently the scattered photon has *less energy* than the incident photon. The energy of the vibration, $\hbar\omega_v$, is $\hbar\omega_v = E_L - E_S$.

Anti-stokes scattering: The molecule relaxes from an excited vibrational state $v = 1$ to its ground vibrational state $v = 0$, leading the scattered photon to have *more energy* than the incident photon given by the energy of the vibration $\hbar\omega_v = E_L - E_S$.

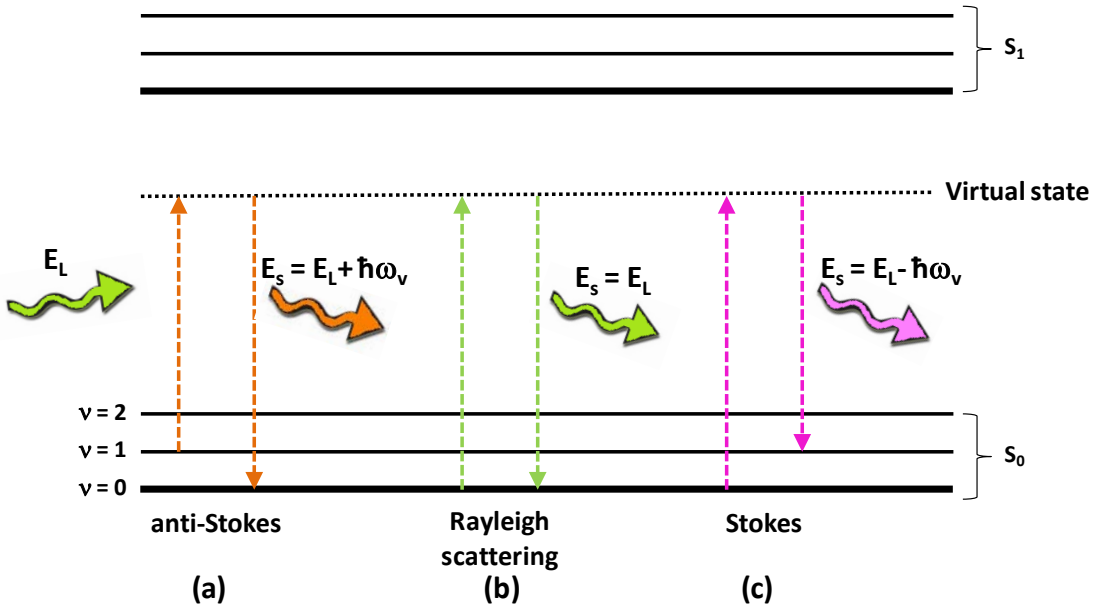

Figure 1.1. Simplified Jablonski diagrams of elastic (Rayleigh (b)) and inelastic Raman scattering (anti-Stokes and Stokes (a,c)) processes.

As noted, for the anti-Stokes scattering to take place the molecule must be in an excited state. According to Maxwell-Boltzman law of distribution of energy, at room temperature 99% of molecules are in lowest possible vibrational state ($v = 0$) therefore there is a greater probability of Stokes scattering to occur over anti-Stokes scattering. As consequence, the anti-stokes side of Raman spectrum is much weaker than Stokes side.

A classical treatment[3,4] of the Raman Effect is depicted in figure 1.2 for a diatomic molecule when an incident electromagnetic wave induces a dipole moment (P). This induced dipole then radiates scattered light, with or without exchanging energy with vibrations of the molecule. The strength of the dipole moment is given by,

$$P = \alpha E \tag{1}$$

whereα is the polarizability of the molecule and E is strength of the applied electric field. Polarizability is defined as a tensor that describes the extent that the molecular orbitals are deformed by the presence of an external field.[5] For the electromagnetic wave, the magnitude vector of the electric field is given by:

$$E = E_0 \cos(2\pi\nu_0 t) \tag{2}$$

whereν_0 is the frequency (Hz) of the incident electromagnetic wave.

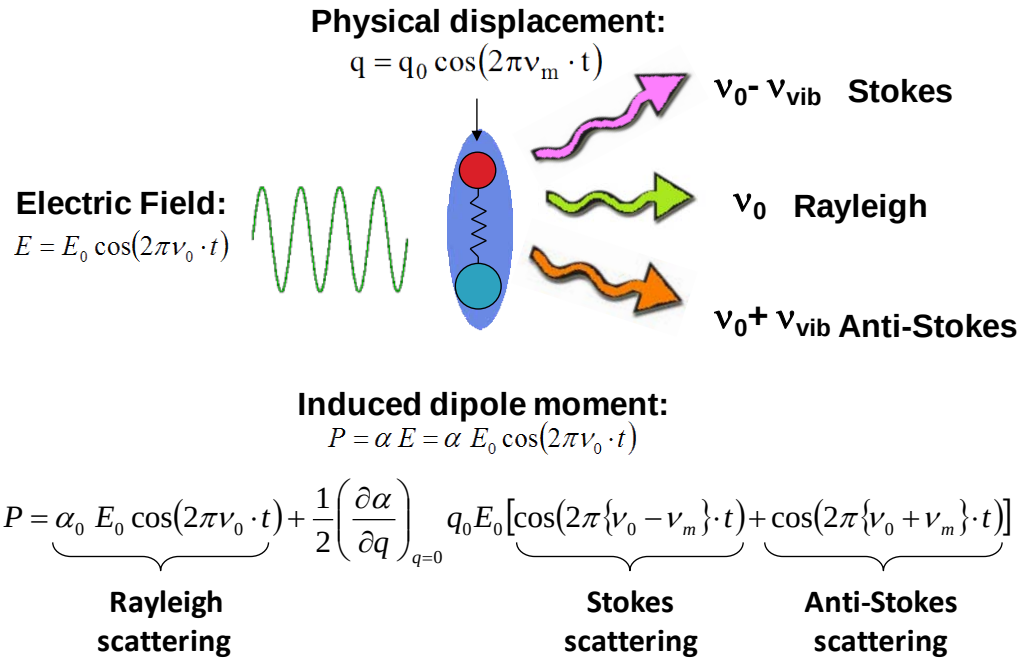

Figure 1.2.Classical description of Raman Effect for a diatomic molecule.

The physical nuclear displacement (q) of atoms from their equilibrium position due to particular vibration with a frequency (ν_m) is expressed as:

$$q = q_0 \cos(2\pi \nu_m t) \quad (3)$$

where q_0 is the vibrational amplitude (maximum displacement about the equilibrium position). If the amplitude of the vibration is small, the polarizability may be approximated by a Taylor series expansion:

$$\alpha = \alpha_0 + \left(\frac{\partial \propto}{\partial q}\right)_{q=0} q + \cdots \quad (4)$$

Taking into account the atom displacement in equation (3),polarizability may be expressed as:

$$\alpha = \alpha_0 + \left(\frac{\partial \propto}{\partial q}\right)_{q=0} q_0 \cos(2\pi \nu_m t) \quad (5)$$

Substituting equation (5) within equation (1) yields:

$$P = \alpha_0 E_0 \cos(2\pi \nu_0 t) + \left(\frac{\partial \propto}{\partial q}\right)_{q=0} q_0 \cos(2\pi \nu_m t) E_0 \cos(2\pi \nu_0 t) \quad (6)$$

Employing the trigonometric identity $\cos\alpha\cos\beta = \frac{1}{2}\{\cos(\alpha+\beta) + \cos(\alpha-\beta)\}$, equation 6 can be simplified as

$$P = \alpha_0 E_0 \cos(2\pi \nu_0 t) + \frac{1}{2}\left(\frac{\partial \propto}{\partial q}\right)_{q=0} q_0 E_0 [\cos(2\pi\{\nu_0 - \nu_m\} \cdot t) + \cos(2\pi\{\nu_0 + \nu_m\} \cdot t)] \quad (7)$$

As noted from equation 7, the induced dipole moment results in radiation in three distinct wavenumbers, ν_0, ν_0-ν_{vib} and ν_0+ν_{vib}. The first term, $\nu_{0,}$ known as Rayleigh scattering corresponds to elastic scattering where the wavenumber is that of the incident light. The latter two terms refer to inelastic processes: ν_0-ν_{vib} is the wavenumber that was down-shifted known as Stokes scattering and ν_0+ν_{vib} is the wavenumber that is up-shifted referred to as anti-Stokes scattering. In order for Raman scattering to take place the external field must induce a change in polarizability along the nuclear mode where $\left(\frac{\partial \propto}{\partial q}\right)$ must be non-zero. If $\left(\frac{\partial \propto}{\partial q}\right)$ iszero, the vibration is not Raman active, therefore this condition can be regarded as the fundamental Raman selection rule.

The use of Raman for routine analytical work has been often limitedby the weakness of the scattering process caused by small cross sections of ~10^{-29} – 10^{-3} cm^2 $molecule^{-1}$. This leads to poor sensitivity, where out of 10^{10} incident photons only one photon will be scattered.

1.2. Surface enhanced Raman scattering (SERS)

Surface enhanced Raman scattering (SERS) has been a technique of intense research during recent years due to its potential to be employed as a powerful qualitative and quantitative tool. This surface method overcomes some of the major limitations of Raman spectroscopy, such as low efficiency of scattering process and low cross sections. Since Fleishman first detected the surface Raman signal from pyridine by use of an electrochemically roughened Ag in 1974,[5] two types of enhancement mechanisms have

been proposed: (1) electromagnetic effect, and (2) chemical effect. Since the induced dipole, P, is denoted bythe product of molecular polarizability (molecular effect) and applied electric field (field effect),

$$P = \alpha E \quad (1)$$

and Raman intensity is proportional to the square of the induced dipole, P, then the enhancement of Raman intensity should be the result of the increase of one of them.[5,7]

The electromagnetic effect, also referred to as field effect, corresponds to "the large local fields the molecule experiences by electromagnetic resonances occurring near metal surface structures."[5] This effect has been widely studied, well understood and has been considered the dominant effect, contributing approximately to a 10^4- 10^8 enhancement.[8] The chemical effect, also referred to as molecular effect, corresponds tothe chemical effect that affects molecular polarizability of a molecule when in presence of a metal surface and is thought to contribute less than 10^2.

1.2.1. Electromagnetic effect of SERS

Electromagnetic enhancement can occur in the presence or absence of a radiation field.[5] The mayor contribution of the electromagnetic enhancement is surface plasmons and is a process that occurs in the presence of a radiation field. Excitation of surface plasmon resonances is induced when incident light induces thecollective oscillation of the conduction electrons in the metal resulting in Raman enhancement. "Large local fields are generated on the surface at plasmon frequency since the metal nanoparticles become polarized. These local fields increase the Raman emission intensity, which is proportional

to the square of the applied field at the molecule. As a result, the effective electromagnetic field experienced by the analyte molecule on these surfaces is much larger than the actual applied field".[5] Surface plasmons can become confined to a nanostructure when its dimensions are much smaller than the incident wavelength (Figure 1.3), resulting in localized surface plasmon resonances (LSPR).[7]

The electrostatic approximation, also known as Rayleigh approximation, is the simplest treatment of the resonance mechanism that accounts for using sharp boundaries and local bulk dielectric functions of the substrate. This approximation is employed for nanostructures with dimensions much smaller than the incident laser wavelength.[5,8] The effective electric field inside the particle E_e in the Rayleigh approximation is given by:

$$E_e = \frac{1}{1+\left[\left(\frac{\varepsilon(\omega)}{\varepsilon_0}\right)-1\right]A} E_{inc} \quad (8)$$

where A is the depolarization factor, E_{inc} is the incident field outside the particle, $\varepsilon_{(\omega)}$ and ε_0 are the dielectric functions of the bulk metal and surrounding medium, respectively. When the denominator of the Rayleigh solution is zero, the resonance of surface plasmons condition is met.When the radius of a sphere is much smaller than the incident laser wavelength, "the electric field is uniform across the particle and the Rayleigh approximation is a good one."[8] The induced field at the surface of the sphere is related to the applied external field by equation (9):

$$E_{induced} = \left\{\frac{[\varepsilon_1(\omega)-\varepsilon_2]}{[\varepsilon_1(\omega)+2\varepsilon_2]}\right\} E_{laser} \quad (9)$$

where$\varepsilon_1(\omega)$ is the complex, frequency-dependent dielectric function of the metal and ε_2 is the dielectric function of surrounding medium (external dielectric constant). This function is resonant at frequency where Re ε_1 = -2ε_2, that is the real part of the dielectric function must be negative and two times the value in magnitude of ε_2.[8,9] At this condition, if the imaginary part of ε_1 (ω) is small then $E_{induced}$ is large.[5] This approximation is for a sphere but has been useful for a wide variety of structures employed for SERS where the numerical value of 2 in the resonance equation will vary for different particles. Large nanoparticle spheres and structures require a complete electrodynamic solution where the electrostatic approximation is not valid.[7]

"The material requirements are to select an excitation frequency for which the real part of the dielectric function (Re ε_1) must satisfy the resonance condition and the imaginary part (Im ε_1) is as close to zero as possible. Imaginary part of the dielectric function of coinage and alkali metals isvery small at resonance frequencies and the resonance condition is met at visible frequencies."[5]

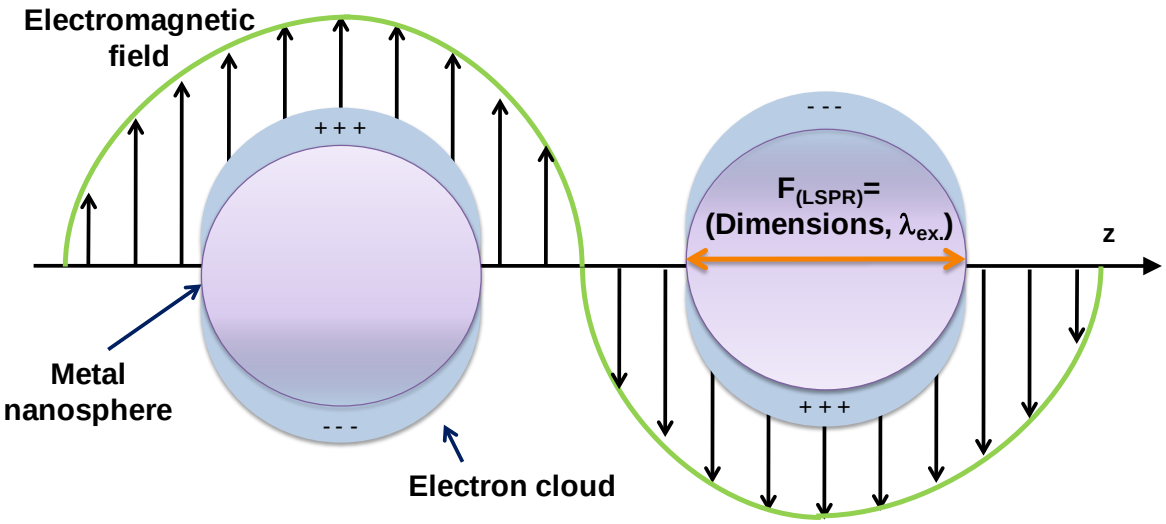

Figure 1.3. Schematic illustration of LSPR excitation.

According to the surface selection rule, the vibrational modes whose polarizability tensor elements are perpendicular to the metal surface should be strongly enhanced in a SERS spectrum.[9]

A molecule within the distance d from the surface of a metallic nanoparticle of radius r;will experience a field E_M,that is the result of superposition of the incoming field E_0 and the field E_{sp} induced by surface plasmon of the metal sphere (figure 1.4).[10] If the scattered Stokes and anti-Stokes field is in resonance with the surface plasmons of the metal sphere, the field will be enhanced.

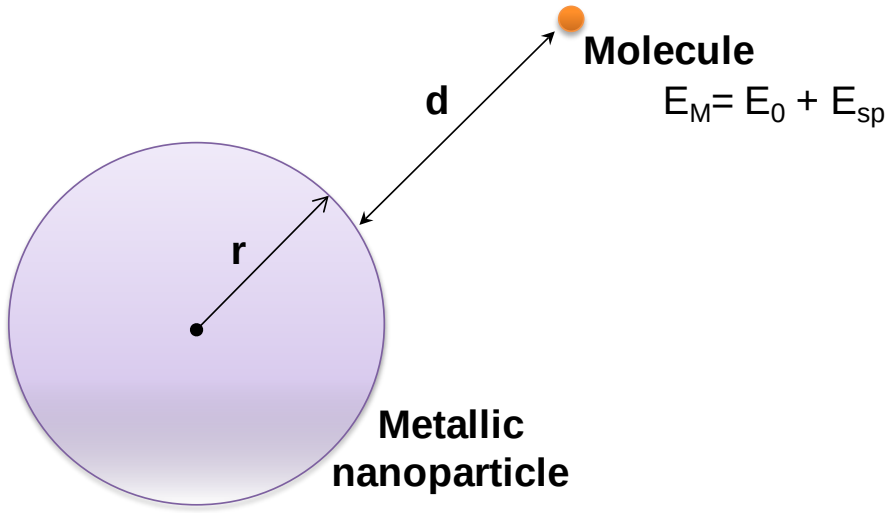

Figure 1.4. Schematic representation of the electromagnetic field experimented by a molecule at a distance d from a metallic nanostructure with radius r.

The electromagnetic enhancement factor for Stokes signal power G(νs), when considering the enhancement effects of the laser and Stokes field is expressed as:

$$G_{em}(\nu_s) = |A(\nu_L)|^2 |A(\nu_S)|^2 \sim \left|\frac{\varepsilon(\nu_L) - \varepsilon_0}{\varepsilon(\nu_L) + 2\varepsilon_0}\right|^2 \left|\frac{\varepsilon(\nu_s) - \varepsilon_0}{\varepsilon(\nu_s) + 2\varepsilon_0}\right|^2 \left(\frac{r}{r+d}\right)^{12} \quad (10)$$

This equation demonstrates that the enhancement scales to the fourth power, E^4, and that this field is strong when the incident and scattered fields are in resonance with the surface plasmons. The electromagnetic field strongly decreases away from the metal surface with growing distance.[8,10] This behavior is described by the dipole decay law, where the enhancement for a single molecule at a distance d from the surface of a nanoparticle with a radius r, as illustrated in figure 1.4, decreases as,

$$G = \left[\frac{r}{r+d}\right]^{12} \quad (11)$$

Similarly, the enhancement of a monolayer of molecules is described as:

$$G = \left[\frac{r}{r+d}\right]^{10} \quad (12)$$

Therefore, the molecule does not have to be in direct contact with the surface to experiment the enhanced local field but within range of the field to polarize the molecule, that is, anywhere within the sensing volume.[5]

1.2.2. Chemical effect of SERS

` Electromagnetic theories do not define the chemical nature of the molecule within their models. However, there is evidence that support that another mechanism, known as the chemical effect, is involved in the SERS effect. It is difficult to treat these mechanisms independently since the effect is multiplicative. Consequently, any experimental parameter that could be probed will influence both mechanisms. Among experimental evidence that suggest this mechanism, SERS intensities obtained for CO and N_2 under the same experimental conditions differ by a factor of 200. This difference is not expected since their polarizabilities are nearly identical and the molecule orientations over the surface are not expected to cause this large intensity difference. Another observation that supports chemical enhancement is potential–dependent chemical experiments.[8,9]

The resonance Raman mechanism mostly supported is that the new electronic states which arise from chemisorption serve as resonant intermediate states in Raman scattering. Chemisorption, illustrated in figure 1.5, is the direct interaction between the molecule and the metallic surface. Such an interaction increases the Raman cross section of the molecule

by charge transfer, where electrons are transferred between the adsorbate and the metal surface. For the adsorbate, the highest occupied molecular orbital (HOMO) and the lowest occupied molecular orbital (LUMO) will be symmetrically disposed in energy with respect tothe Fermi level of the metal. Transfer excitations can occur at about half the energy of the intrinsic intramolecular excitations of the adsorbate. These states are spatially localized, where changes in Fermi energies without affecting the adsorbate orbital energies will cause shifts in the wavelength of the charge transfer transition. Therefore, evidence of dynamic or photon driven charge transfer could be obtained by perturbations that affect only the Fermi energy. The relation between the applied change in the Fermi energy and the shift in transition energy provides the direction of the charge transfer, where a red shift indicates an increase in Fermi energy and the charge transfer occurs from filled metal orbitals to empty adsorbate orbital.[8,9,2] Chemical enhancement occurs upon modification of the Raman polarization tensor upon adsorption of the molecule onto the molecule surface.

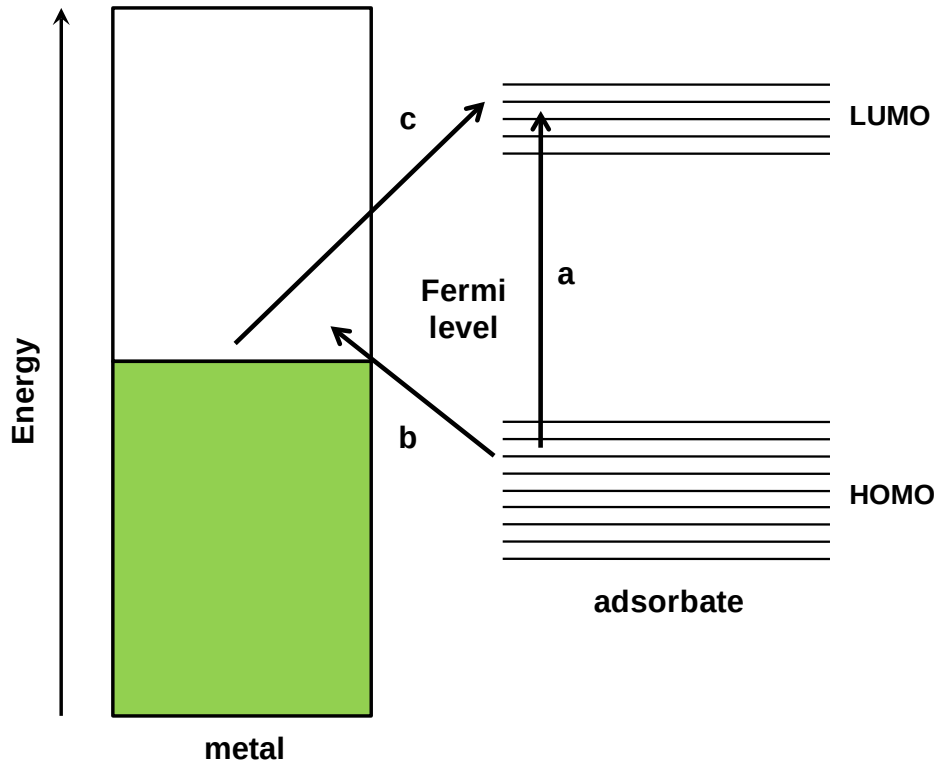

Figure 1.5. Schematic representation of the charge-transfer mechanism. There are two possible scenarios, where the laser energy can be (a) in resonance with an electronic transition of the molecule-metal complex; or (b,c) can profit from an indirect coupling (charge transfer) through the metal.

Hence, SERS also provides a mean to effectively study the binding and chemical orientation of adrug with respect to the metal surface. This can be assessed by monitoring changes in the relative intensities and Raman shifts of the corresponding analytes which can interact with the metal surface by two plausible processes: (1) Physical adsorption: a reversible attachment to the surface and (2) Chemisorption: a covalent binding to the surface. SERS studies performed by Fleger et al. demonstrated that monitoring either the

presence or absence of red shifts between SERS and Raman spectra for crystalline compounds can serve as an indicator of the molecule orientation with respect to the metal surface as well as to provide structural details on the nature of the adsorbate to surface binding.[11,12] SERS can also provide information of interfacial processes, which can be used as a model system for the study of antimicrobial drugs within liquid and solid interphases..

1.2.3. Enhancement factors

SERS enhancement factor is one of the most important figures of merit when characterizing the SERS effect and when comparing results to theoretical calculations by specialized software. The concept of SERS enhancement factor results from the increase in signal resulting from the increase of cross section of the molecules. Enhancement factors of 10^7-10^8 can be sufficient for single molecule detection where the maximum magnitude ranges among 10^{10}-10^{14} under optimized conditions. SERS conditions, such as substrate, analyte, excitation wavelength, etc., affect the enhancement factors.[13]

Overall enhancement, that is electromagnetic and chemical mechanisms, can be determined experimentally by determining SERS and NRS (normal Raman scattering) intensities for an analyte. The intensity of NRS scattering is given by equation (13),[7]

$$I_{NRS} = K(\upsilon) \times N_{NRS} \times \frac{\partial \sigma}{\partial \Omega} \times I_{0,NRS} \times \upsilon^4 \times t_{NRS} \qquad (13)$$

where $K(\upsilon)$ is the instruments response factor, N_{NRS} is the number of molecules in the probe volume, $\frac{\partial \sigma}{\partial \Omega}$ is the differential cross-section of the molecule, $I_{0,NRS}$ is the laser

intensity, υ^4 is the frequency dependence of the scattering process, and t_{NRS} is the acquisition time. Similarly, the SERS scattering intensity is given by equation (14),

$$I_{SERS} = K(\upsilon) \times N_{SERS} \times \frac{\partial \sigma}{\partial \Omega} \times I_{0,SERS} \times \upsilon^4 \times t_{SERS} \times EF_{SERS} \qquad (14)$$

where, as noted, I_{SERS} is similar to I_{NRS} except I_{SERS} is multiplied by an enhancement factor (EF_{SERS}) factor. $K(\upsilon)$andυ^4 are constants if the collection geometry and the same excitation frequency is used. When the intensities are normalized for laser power and acquisition time the ratio of the two intensities can be rearranged as equation (15),

$$EF = \frac{I_{SERS}/N_{surf}}{I_{vol}/N_{Vol}} \qquad (15)$$

Equation (15) is commonly employed to determine average SERS enhancement factor across different substrates.[13]The value of EF employing this equation represents the overall enhancement in Raman scattering for molecules within close proximity to the surface of the plasmonic surface. A common difficulty in determining the EF is the determination of the number of molecules that give rise to the enhancement.

1.3. Plasmonic substrates

Substrate fabrication has been the key issue in the last years involving SERS applications since plasmonic response as well as signal reproducibility are strongly dependent of their surface morphology characteristics. Since investigators such as Fleischman, Hendra, and McQuillan;[6]Jeanmarie and Van Duyne[14],and Albrecht and

Creighton[15] observed the SERS effect, nanoparticles, such as colloidal nanoparticles, have been extensively employed as plasmonic substrates for surface enhanced Raman scattering (SERS) applications. In the mid 1980's, there was a loss of interest in SERS due to limited reproducibility rendered by colloidal metal nanoparticles, the most commonly used substrates at the time.[16] Furthermore, the SERS effect had only been obtained for highly polarizable small molecules and most analysis were carried out at above trace level detection limits (10^{-1}-10^{-3}). Renewed attention toward SERS raised in 1984, when solid substrates consisting of nanospheres or nanoparticles covered with a nanolayer of metal was used as a general applicability SERS substrate for the trace organic detection.[17]Since then, substrates have evolved from traditional substrates such as electrochemically roughened electrodes and colloidal suspensions to more elaborate substrates where specific nanostructures are fabricated directly on the surface attained by nanolithographic techniques such as, nanosphere lithography (NSL), nanoimprint lithography (NIL) and electron-beam lithography (EBL).[17,18,19] These advances have developed toward the goal of engineering plasmonic substrates that render increased signal responses, high reproducibility and ultratrace detection of target analytes for a wide variety of applications.

1.3.1. Colloidal nanoparticle solutions

Colloidal nanoparticle solutions have been traditionally employed as SERS substrates since they render increased enhancement factors as well as offer ease in fabrication, and good stability.These are commonly fabricated by wet chemistry synthesis which can attain a wide array of possibilities as to the shapes and sizes of nanoparticles that can be achieved.[19] In addition, straightforward characterization of colloidal solutions is

possible by UV absorption.[5]Notwithstanding these advantages, the synthesis procedures often lack reproducibility from batch to batch where tedious processes to attain optimal sizes are required. In order to use colloidal nanoparticles as SERS substrates, aggregation must be induced by the addition of salts or the analyte leading to the formation of faceted or aggregation of two or more nanocrystals. Even though aggregation limits the reproducibility of SERS signal enhancements, it leads to the formation of "hot spots".[19]

Colloidal metallic nanoparticles can be synthesized by chemical reaction, laser ablation and photoreduction. The most commonly employed is chemical reaction that is based on the reduction of metal salts with reducing and capping agents. Certain parameters must be controlled in order to achieve specific size, size distribution and aggregation such as reaction temperature, pH, type of metal salt, reductant and surfactant. On the other hand, "chemically pure" colloidal solutions can be obtained by use of laser ablation and photoreduction methods where the effect of residual ions in resulting spectra is reduced.[9]

1.3.2. Immobilized metallic nanoparticles

The reproducibility issue encountered by use of colloidal solutions can be mitigated by immobilizing metallic nanoparticles on a solid support. Island films are the simplest nanostructured substrates which are constructed by the electro-deposition of thin metallic films of thickness under 10 nm on a solid support such as glass. The thickness of the deposited film plays an important role in the shape and size of the resulting metallic nanostructures. Metal deposition can be attained by physical vapor deposition and sputtering.[20]

Silver/polydimethylsiloxane (Ag/PDMS) nanocomposites are an example of these substrates. These are simple, low cost metal/polymer nanocomposites that are metalized by physical vapor deposition (PVD). Rendered nanoparticles are distributed just below the surface as embedded clusters or isolated nanoparticles resulting in fractal-like surface morphologies.Their optical and sorptive properties make them a broad spectrum SERS substrate for the detection of small aromatic molecules particularly aromatic acids.[21]The immobilization of the silver particles within the PDMS matrix inhibit the rapid oxidation of nanometallic silver and reduces the number of experimental variables facilitating the study of metal adsorbate interactions.

Substrates can be metalized by physical vapor deposition processes such as vacuum evaporation, sputter deposition, ion platting and arc vapor deposition. PVD processes consist of the deposition of a material by vaporizing atoms or molecules from a solid or a liquid source, the vapor is then transported through a vacuum to the substrate where it condenses. Films from a few Å to thousands of Å can be obtained. The most economical of these processes is vacuum evaporation, where almost any inorganic or organic material can be deposited by a pollution free process. Thermal evaporation is the process in which a material, placed in a evaporation source, reaches the substratewithout collision of the molecules while transporting from the source to the substrate.[22, 23] This process is characterized by poor step coverage and shadowing effects illustrated in figure 1.6.

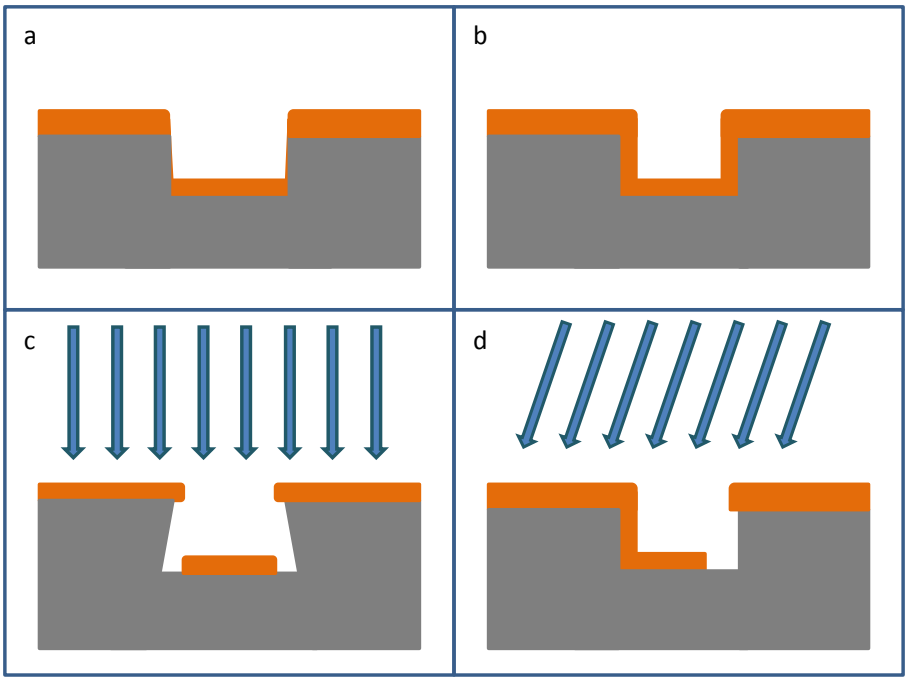

Figure 1.6. Representation of the deposition processes in thermal evaporation: (a) Poor step coverage; (b) good step coverage; (c,d) shadow effects. Arrows represent the trajectory of deposited material.

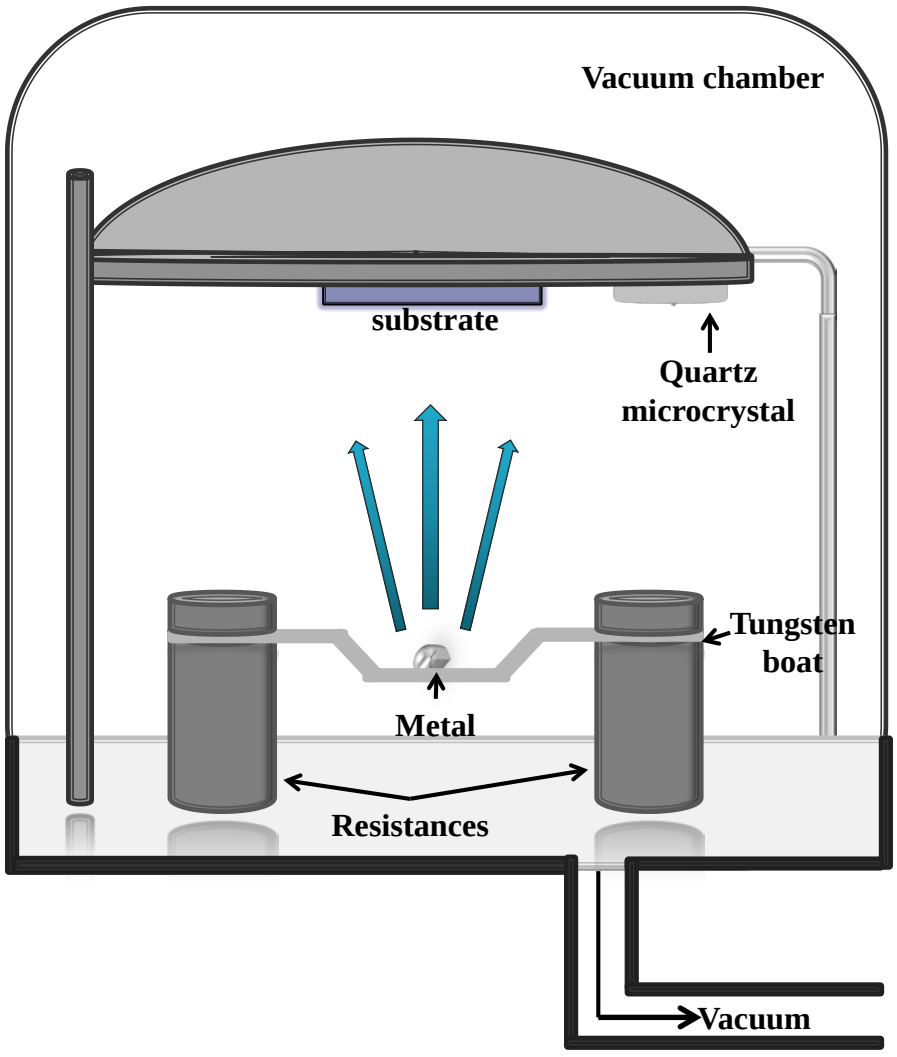

Figure 1.7. Schematic illustration of a physical vapor deposition (PVD) chamber.

1.4. Nanolithography

Although immobilized nanoparticle substrates have proven effective for the reliable detection and characterization of small aromatic molecules, they are limited for reproducible quantification due to their inhomogeneous surface. Nanofabrication

techniques have been widely exploited for the design and development of innovative SERS substrates due to their potential to provide nanostructures directly on a solid support with fine control over specific geometric features, sizes, orientation and interparticle spacing of nanostructures. Control over such parameters allows the possibility of substrate tailoring for specific excitation wavelengths. Nanolithography has led to the nanotechnology revolution and refers to "the ability todefine patterns on surfaces at ever-decreasing length scales".[22] The most employed technique involves the exposure of resist materials to energetic photons or particles to prompt structural/chemical modifications to induce a change in the solubility of the exposed areas of the resist when placed in a developing solution. The solubility of the exposed areas of the resist will be different than areas that were not exposed. When the exposure results in an increase in solubility, the resist is known as positive tone resist; on the contrary when a decrease of solubility is obtained the polymer is a negative tone resist. Upon exposure of a positive tone resist to the radiation, the bond of the backbone of the polymer breaks decreasing its molecular weight, on the other hand, when negative tone resists are exposed cross-linking of the polymer occurs increasing its molecular weight. Resist exposure can be achieved by serial (direct) or parallel modes. Serial refers to the exposure of the resist point by point where the lithographic definition is defined by the diameter of a focused beam. The exposure in parallel mode is achieved by the use of masks, where the image is transferred to the resist by projection, contact or proximity alignment.

Among nanolithographic methods, electron beam lithography (EBL) has ledthe construction of a broad diversity of plasmonic SERS-active substrates with unique

characteristics. Moreover, the combination of EBL liftoff protocols and reactive ion etching (RIE) have proven effective on the fabrication of robust, more durable, periodic plasmonic nanoarrays.[17,19] To this date, the majority of the EBL and RIE work has been focused on the construction of extended nano-arrays of a single geometrical pattern and morphology, such as diffraction gratings with simple ridges and grooves,[17, 19] or more complex diffraction pillars.[24, 25]

1.4.1. Electron Beam lithography (EBL)

Electron beam lithography can be achieved by different modes, such as direct write electron beam lithography (EBL) and electron beam projection lithography (EPL). EBL has been widely employed for the fabrication of nanostructured SERS substrates and is based on writing a specific pattern onto an electron sensitive resist, which is spin coated onto a Si wafer, by exposing the substrate to a small electron beam (10 nm or less) with Gaussian profile intensity produced by the microscope (Gaussian beam system).[18]

Early instruments consisted of scanning electron microscopes (SEM) adjusted to write a pattern by control of a computer or a flying spot scanner. In the system, an electron beam is generated by a thermionic emission filament or a field emission tip which is shaped and focused into a spot by magnetic lenses and apertures. Electrostatic coils and/or magnetic coils deflect the beam where one of the deflectors turns the beam on and off according to the pattern and the other deflectors scan the beam across the surface of the substrate. Therefore, the pattern is obtained by scanning the beam over the substrate in a raster pattern

while the beam is turned on and off according to the pattern. To cover an entire area with patterns, a combination of mechanical sample motion and deflectors is used.

High resolution, approximately of 20 nm, is attainable with EBL. Furthermore, it does not require the use of masks as required in photolithography, decreasing costs. Patterns can be generated in software programs such as AutoCAD, where they can be easily modified and optimized. The final spot size is affected by the following four factors: effective source, chromatic aberration, geometric aberration and space charge effects, where the net beam is estimated as the square root of the sum of squares of main contributors. One limitation of this technology is the extended exposure times. These are dependent of the sensitivity of the resist and the total beam current on the sample. Low beam currents result in better resolution and finer spot size, however the exposure time increases.

Many systems have been developed towards the aim of increasing throughput. Shaped beam systems (1970) where established to attend this aspect.However the system results in poor resolution when compared to Gaussian beam systems. Therefore, Gaussian systems remain more generally used where a compromise between time and resolution is met. Another system is the cell or character projection beam system that ismainly employed for advanced development and prototyping where larger features are used, and results in modest throughput.

1.4.2. Reactive Ion Etching (RIE)

After substrate developing, etching and lift-off are common follow up procedures to generate the nano-arrays. Reactive ion etching is a type of dry etching process that

combines physical and chemical processes. This process consists of the use of plasma, where the collisions of the incident ions within the plasma "activate" the surface of the material. Reactive species then react only with activated surfaces. Fast etching rates in the vertical position are obtained with RIE since the directionality of the ions velocity results in more collisions in the horizontal surface rather than the walls.[23]Thepattern is engraved into the substrate resulting in the formation of pillars within the substrate surface. Then, the remaining resist from the development process is removed and the metal film is deposited over the substrate. The metallic nanostructures are obtained as a continuous film. On the other hand, lift-off processes involve the deposition of a metal film over the developed substrate and finally the resist is removed. Discrete metallic nanoparticles are generated employing this method. Substrates fabricated by etching render improved SERS performance over lift-off generated substrates since coupling between particles is not favored by the free metal spacings in the substrates attained by lift-off. In addition, RIE resulted in higher reproducibility and spatial uniformity of patterns over lift-off procedures.[19]

High durability substrates can be attained by EBL/RIE processes, whereas with proper handling, the nano-arrayed substrates can be cleaned and reused several times as SERS substrates. EBL/RIE fabricated substrates can also be employed as stamps or molds in nanotransfer printing (nTP), a simple stamping technique that involves the transfer of features on a stamp to a substrate with high resolution.[26,27] This nanofabrication technique has proven the ability of fine control over fabrication parameters and reproducibility in the construction of nanostructured substrates over extended areas. The combination of these

nanofabrication techniques with combinatorial spectral mapping has proven efficient in the fabrication of aggregate like nanostructured substrates.[28]

1.4.3. Nanofabrication parameters

Fine control over metallic nanoparticle shape, size, aspect ratio, interparticle spacing and geometrical arrangement by EBL in the development of SERS substrates have resulted in the fabrication of a wide diversity of ordered nano-arrays with unique and specific characteristics. This nanofabrication technique has also allowed the performance of extensive systematic studies to determine the impact these parameters have on SERS signal intensities. Studies by De Jesús et al.[29] on densely packed polymeric periodic arrays demonstrated the effect that different geometrical shapes have on SERS signal enhancement whereas shapes such as ellipses and hexagons have been proven to render large SERS signal enhancements over square and triangular shapes employing 633 nm. This was justified by the increase in packing density and increase in number of loci per nanoparticle. In addition, it was found that particle symmetry also has an important effect in the resulting signal enhancement where the generation of LSPs and the magnitude of the SERS signal are affected by the orientation of the excitation polarization vector relative to nanoparticle axis and very small interparticle spacing. These two factors also have an influence on the coupling of the LSPs. Closely-packed periodic arrays of elliptical disks fabricated by EBL were employed by Oran et al.[30] to study the effect of varying gap of elliptical dimers arrays (20- 100 nm) as well as the effect of aspect ratio on substrate performance. They found that experimental data differed from theoretical predictions, whereas their results demonstrated that as the interparticle spacing (gap) increased the

resulting SERS intensities increased as well. However, arrays with close gap demonstrated high variability in comparison to those with increased gap due to limitations in resolution from the EBL system, and therefore the effect could not be studied. The aspect ratio for the elliptical nanoparticles influenced the SERS signal enhancement whereas oblate features rendered improved signal enhancement over prolate ellipses. The advantages of EBL have also led efforts toward the development of substrates with particle aggregates that mimic the randomness of colloidal nanoparticles within colloidal solutions toward the end of generating hot spots. Wells et al.[28] proved the ability to fabricate reproducible, well defined complex patterns comprised of particle aggregates with random distribution and orientations that resemble colloidal aggregates employing EBL/RIE. The use of combinatorial spectral mapping allowed the identification of specific cells within the array that render high SERS performance where once identified these were repeated over extended areas. Enhancement factors of $5x10^8$ were reported for substrates with specific cells that were reproduced uniformly over extended areas.

1.5. Electromagnetic numerical tools: Finite-Difference Time Domain method

One advantage of nanolithographic techniques in the fabrication of plasmonic substrates is the construction of specific, well-defined nanostructures which allows the effective simulation of theoretical models of their electromagnetic fields employing numerical tools. There are two groups of numerical tools: Partial differential equation solvers and semi-analytical methods.[2] Finite differential-time domain (FDTD) and finite-elements methods

(FEM) are examples of partial differential equation solvers. These methods solve Maxwell's equations numerically using standard techniques that have been developed to solve partial differential equations with appropriate boundary conditions. Mathematical methods and solvers used in these methods are highly optimized and tested since they have been developed by mathematicians, computer scientists and physicists. However, they are not optimized for specificity of EM problems. Semi-analytical methods are specifically developed for electromagnetic (EM) problems, Maxwell's equations solvers and use analytical tools to reduce computing requirements. Discrete dipole approximation (DDA) and multiple multipole (MMP) method are examples of these methods. These methods require complex implementation and user expertise (large user input and solid knowledge on the method).

As previously mentioned, two representative methods of direct numerical solutions are FDTD and FEM. The main differences between them are the way the differential equation is actually solved and the physical difference equation that is solved. FDTD methods solve the time dependence fields whereas FEM methods solve the frequency dependent fields. FDTD methods consist in using the finite-difference approach to solve the time dependent Maxwell's equations under a prescribed exciting field. "The excited field can be a single short pulse where the response to the pulse has information on Fourier components of the field at all frequencies. The response of the system at all frequencies can be computed from a single time dependent calculation followed by appropriate Fourier transforms."[2] Many SERS and plasmonic applications require elaborate meshes increasing the complexity of the method.

1.6. Statement of the problem

Unequivocal identification of pharmaceutical and personal care products (PPCPs) in environmental matrices at trace levels plays an important role in environmental sciences. PPCPS have been considered an emerging pollutant since their constant release by anthropogenic sources increases their persistence into the environment. In addition, these have been found in soil and water bodies, such as superficial and underground water at trace levels, ppb (μg/L) and ppt (ng/L). This group is composed of controlled and over-the-counter (OTC) drugs, veterinary drugs, cosmetics, soaps and fragrances, among others. Within PPCPs, veterinary drugs, such as 4-arsanilic acid, roxarsone and acetarsone, have emerged as an environmental concern since their use is associated to the discharge of the intact druginto poultry litter. Some of the main causes of concern include the release of inorganic arsenic ions, As^{+5} and As^{+3} due to degradation procedures and the increased solubility of the drugs and their metabolites increasing their mobility in the environment toward soils and water bodies. Detection and study of these pollutants rely heavily on chromatographic methods and inductively coupled plasma coupled to mass spectrometry. Even though these techniques have proven useful over the years these result in costly operational procedures, sample destruction, increased amounts and preparation of sample, and complex-time consuming procedures. Hence, there is the need to develop simple, non-destructive, information rich detection schemes to facilitate the rapid and cost-effective detection of antimicrobials drugs and their byproducts.

Surface enhanced Raman scattering (SERS) has been considered an attractive alternative for qualitative and quantitative analysis of bioactive agents and emerging

pollutants in aqueous media. This surface method overcomes some of Raman spectroscopy's major limitations, such as low efficiency of scattering process and low cross sections while maintaining its main advantages of unequivocal identification due to large amount of structural information rendered, low sample requirements and trace detection limits attainable. The use of metallic nanostructures generates a secondary electric field which adds on to the incident field when conduction electrons of the metallic nanostructure are displaced in the same frequency oscillations as the incident light. This effect creates surface plasmons.[1, 2] When the size of the nanoparticles are smaller than the incident wavelength, the light wave becomes trapped generating localized surface plasmons.[7] Nonetheless, the implementation of SERS as a quantitative tool has often been limited by the response of traditional plasmonic substrates employed. The development of new innovative plasmonic substrates that render reproducible, enhanced and tailored signal responses have been an area of intense research. Most studies are based on substrates with periodic nano-arrays where simple parameters are optimized toward the result of increased SERS enhancement signals.

This work aims at the design, development and application of random metal/polymer nanocomposites and plasmonic hybrid nano-arrays for the detection, characterization and quantification of antimicrobial drugs in aqueous media. Low cost Ag/PDMS nanocomposites are employed for the unequivocal identification of selected veterinary antimicrobials at trace levels by surface enhanced Raman spectroscopy for the first time. In addition, an assessment of the molecular orientation of the compounds with respect the metallic surface was accomplished. Specialized hybrid nano-arrays were

fabricated to perform at multiple wavelengths serving as a versatile substrate. The impact that simple fabrication parameters, such as orientation and interparticle spacing of nanostructures composing the arrays, has on signal enhancement was assessed.

CHAPTER 2

SURFACE-ENHANCED RAMAN SCATTERING (SERS) CHARACTERIZATION OF TRACE ORGANOARSENIC ANTIMICROBIALS USING SILVER/POLYDIMETHYLSILOXANE NANOCOMPOSITES

This chapter is a revised version of an article under the same name published in Applied Spectroscopy by Jenifier Olavarría-Fullerton, Sabrina Wells, William Ortiz-Rivera, Michael J. Sepaniak and Marco A. De Jesús.

Olavarría-Fullerton, J.; Wells, S.; Ortiz-Rivera, W.; Sepaniak M.J.; De Jesús, M.A.; Surface enhanced Raman scattering (SERS) characterization of trace organoarsenic antimicrobials using silver/polydimethylsiloxane nanocomposites. *Appl. Spectrosc.* **2011,** *64(4)*, pp 423-428.

My primary contributions to this article were: (A) Design of the project and development of experimental protocols to employ SERS in the qualitative analysis of organoarsenic drugs, (B) design and fabrication of metalized/PDMS nanocomposites, (C) collection and interpretation of most of the analytical data, (D) collection and interpretation of cited data, and (E) most of the article write up.

2.1. Introduction

Veterinary antimicrobials such as 3-nitro-4-hydroxyphenylarsonic acid (roxarsone), 3-acetamido-4-hydroxyphenylarsonic acid (acetarsone), and 4-aminophenylarsonic acid (4-arsanilic acid) are currently used in the vast majority of US broilers as an effective treatment against coccidiosis while improving growth, pigmentation, and feed efficiency when administered as regulated by the U.S. FDA (21 CFR 558.30; Code of Federal Regulations).[31] Once ingested by the animal, over 90% of the drug appears to be excreted unchanged.[32] According to the most recent report of the USDA, the US produced 8.285 billion broiler chickens in 2009 from which a significant number are still fed with roxarsone.[33] A previous

study of poultry litter from the Southeast US, showed a total As concentration in the range of 1–39 mg/kg dry weight, with a water solubility in the range of 70-95%.[34] The relatively high solubility of these drugs and the increased use of poultry liter as land fertilizer have raised concern on the potential health impact of organoarsenics antimicrobials as they percolate from litter to water and soil.[32, 35] Photolytic and biodegradative processes involving these drugs are the main source of concern since they can result in the release of toxic arsenic species as well as promoting the expression of bacterial strains resistant to existing antimicrobial agents.

Stolz and collaborators have investigated the biotransformation of roxarsone by *Clostridium* strains which are commonly found in avian litter under anaerobic conditions.[36] They reported 3-amino-4-hydroxybenzenearsonic acid and inorganic arsenic are the main degradation products of roxarsone (figure 2.1) in fresh litter, while As^{V} was the only species present after extended microbial action. Analysis of roxarsone in methanogenic sludge from wastewater treatment facilities confirm the reduction of the nitro-group of the drug, as well as, the presence of both As^{v} and As^{III} species in the effluent media.[37] Research conducted by Rosal et al. have also shown that photodegradation plays an important role in roxarsone reduction of its nitro group and the release of arsenate (AsO_4^{3-}).[38]

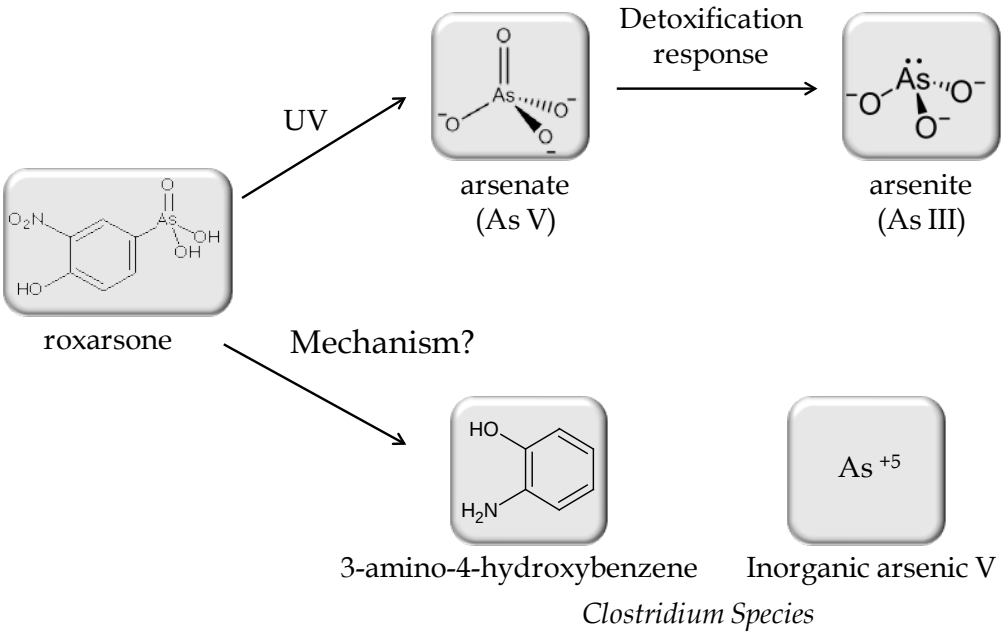

Figure 2.1. Proposed degradation processes for roxarsone.

Current methods to detect organoarsenics rely heavily on hyphenated-mass spectrometric techniques like high performance liquid chromatography (LC-MS) and inductively coupled plasma with mass spectrometry detection (ICP-MS).[35, 36, 39] Additional techniques like multi-detector gas chromatography, capillary electrophoresis-mass spectrometry (CE-MS) and ion chromatography with inductively coupled plasma-mass spectrometry (IC-ICP-MS) have also been employed in the study of organoarsenic speciation.[37-40] Notwithstanding their usefulness, the abovementioned techniques are costly, sample destructive, and require complex and time-consuming operational and preparation protocols. Hence, there is the need to develop simple, non-destructive, information rich detection schemes to facilitate the rapid and cost-effective detection of antimicrobials drugs and their byproducts.

The low polarizability of water combined with advances in vibrational microscopy and laser technology have made Raman spectroscopy a promising tool for the analysis of drugs and bioactive agents in aqueous media.[1] The technique is particularly attractive for the analysis of antimicrobials due to its scalability for field operations, low sample requirements, and amount of structural information it provides. Nevertheless, the use of Raman for routine analytical work has often been limited due to its small scattering cross-sections (low sensitivity) and the potential for thermal and photolytic decomposition of the sample by the Raman excitation source. The sensitivity issue can be addressed by using surface methods such as surface enhanced Raman scattering (SERS).[1, 6] SERS is induced by the excitation of localized surface plasmon resonance (LSPR) at noble metal nanostructures, which augments the effective Raman cross section of molecules within close proximity to the metal surface. The enhancement enables the sub-micromolar quantitation of a variety of chemicals with potential for single molecule detection for selected systems.[41, 42]

Over the last decade improvements in SERS substrates have led to an evolution from conventional nanostructures like those from silver islands on glass[5], colloidal silver solutions[43], colloidal particles encapsulated in sol-gels[44], to more modern, yet economical and reproducible substrates such as Ag/PDMS and Au/PDMS nanocomposites.[45,46] Although considerably more expensive, lithographically engineered substrates have also gained much attention due to the its enhanced sensitivity and ability to fabricate ordered[29, 30] and random like substrates[28], whereas parameters such as varying aspect ratio, control of shapes and sizes of arrayed features and density packing, allow for substrate tailoring. Ag/PDMS optical and sorptive properties make them a broad spectrum SERS substrate for the detection of small aromatic molecules particularly

aromatic acids.[45] The selectivity and increased performance of this composite material toward aromatic acids makes it an attractive candidate for the SERS detection of arsenic antimicrobials in water and other environmentally relevant media.[47] The immobilization of the silver particles within the PDMS matrix also reduces the number of experimental variables facilitating the study of metal adsorbate interactions.

Raman spectroscopy also provides a mean to effectively study the binding and chemical orientation of the drug with respect to the metal surface. This can be assessed by monitoring changes in the relative intensities and Raman shifts of the corresponding antimicrobials which can interact with the metal surface by two plausible processes: (1) *Physical adsorption:* a reversible attachment to the surface and (2) *Chemisorption:* a covalent binding to the surface. SERS studies performed by Fleger et al. demonstrated that monitoring either the presence or absence of red shifts between SERS and Raman spectra for crystalline compounds can serve as an indicator of the molecule orientation with respect to the metal surface as well as to provide structural details on the nature of the adsorbate to surface binding.[48, 49] SERS can also provide information of interfacial processes, which can be used as a model system for the study of antimicrobial drugs within liquid and solid interphases, as well as provide potential degradation products and their environmental fate.

This work uses SERS as an analytical tool for the rapid characterization and identification of the veterinary antimicrobial roxarsone, 4-arsanilic acid and acetarsone in water, using Ag-PDMS as SERS-active substrates. The 792 cm^{-1} stretching band of the arsonic acid is used as a positive identifier for arsenic acids. Unequivocal identification of each analyte within the arsenic antimicrobial series was performed by monitoring the fingerprint region of the spectra. The

sorption and chemical orientation of the analyte with respect to the silver surface is discussed. The benefits of the technique for the study of antimicrobial agents in environmental samples are also presented. Spectral differences, such as appearance and absence of peaks, as well as red shifts in SERS spectra with respect to Raman spectra are discussed.

2.2. SERS substrate preparation

PDMS substrates were prepared by carefully mixing a 1:10 mass ratio of Sylgard-184 elastomer (Dow Corning) with its curing agent. The PDMS mixture was carefully degassed for 15 minutes to remove any residual air from the matrix and then casted in polystyrene petri dishes and cured in the oven for 30 minutes at approximately 80^{o}C. Once hardened the PDMS slabs was removed and stored at room temperature for 24 hours until they reach full mechanical strength.

2.2.1. SERS active substrate

The PDMS surface was metallized under vacuum ($1.0x10^{-6}$ (±0.2) torr), in an electrothermal evaporator (Cooke Vacuum Products, Inc.). The thickness of the metal coating was registered in a quartz analytical microbalance integrated on the system. The evaporation was performed with standard Ag shots (99.9999%, ACROS) at a rate of approximately 1.0(±1) Å/s. Thickness of the SERS active surface was in the range of 20 (±2) nm. After deposition, all substrates were placed under vacuum and in dark conditions for further analysis.

2.3. Sample preparation

Roxarsone (98%) and 4-arsanilic acid (99%) were purchased from Acros Organics. Acetarsone (98%) was purchased from MP Biomedicals. Neat laboratory samples of each analyte were prepared on capillary tubes and used as standard reference materials. One millimolar stocks of each analyte were prepared by dilution in 18 MΩ deionized water (Barnstead, Co.). A 50 µL aliquot of a $1.0x10^{-4}$ M laboratory sample containing each antimicrobial as used on the SERS studies.

2.4. Instrumentation, data acquisition and analysis

All Raman spectra were acquired in a LabRam-HR Microscope from JY-Horiba. The instrument uses an Olympus BX-40 microscope with an infinity-corrected 10X objective that delivers 5.0(±0.1) mW of the 632.8 nm line of a He-Ne Laser. Spectra were acquired in a 180° scattering geometry using a computer controlled x-y-z stage to focus the incident laser beam. Conventional Raman spectra of the solids were collected with an acquisition time of 7 seconds intervals, while all SERS spectra were collected with 1 second acquisition time. All spectra were baseline corrected in order to compensate for baseline drift due to changes in refractive index. The Raman spectra of the analytes were collected by mapping a 250x250 µm area of the SERS active substrate at 50 µm intervals for a total of 25 data points (N=25).

2.5. Safety considerations

Special care must be taken when handling arsenic compounds since they are considered carcinogens, and potentially toxic via inhalation, ingestion and skin contact. Appropriate safety equipment, such as chemical safety goggles, nitrile gloves and lab-coat must be used at all times while handling these compounds, as well as, adequate ventilation. Wastes must be disposed in its corresponding hazardous waste container.

2.6. Results and discussion

The sorptive enrichment of small aromatic molecules by partitioning into PDMS has been used in a variety of techniques including solid phase micro extraction and rotative sorptive extraction.[50] In its native state, PDMS contact with aqueous solutions result in the sorption rather than adsorption of low molecular weight organic compounds that can be selectively distributed by adjusting simple experimental variables such as pH and ionic strength.[45, 51] Metallization of PDMS by electro-thermal evaporation is a cost effective process to fabricate reproducible and durable SERS substrates. PDMS properties as a solid phase extractor serve to augment the effective concentration of a broad range of small aromatic molecules, including organic acids near the metal surface improving the sensitivity of the SERS active surface.[29, 45] Moreover, the low dielectric properties of the polymer can influence the excitation of the localized surface plasmon (LSPR), of the metal nanoparticles and provides a reducing environment that inhibits the rapid oxidation of the silver, therefore extending the shelf life of the constructed substrate. PDMS ability to extract aromatic acids makes it an ideal candidate for the characterization of trace organoarsenics in aqueous environments.

From a structural standpoint, the molecular structures of organoarsenic antimicrobials are of low symmetry. For instance, the 4-arsanilic acid has Cs symmetry whereas both roxarsone and acetarsone belong to the C_1 group. According to the corresponding character table, 4-arsanilic acid will exhibit 29a' (planar) and 24a'' (non-planar) Raman active modes.

2.6.1. Characteristic group frequencies of antimicrobials

All antimicrobial drugs selected in the study contain the arsonic acid group in its molecular structure (figure 2.2), that contributes to the biological activity of the drug.

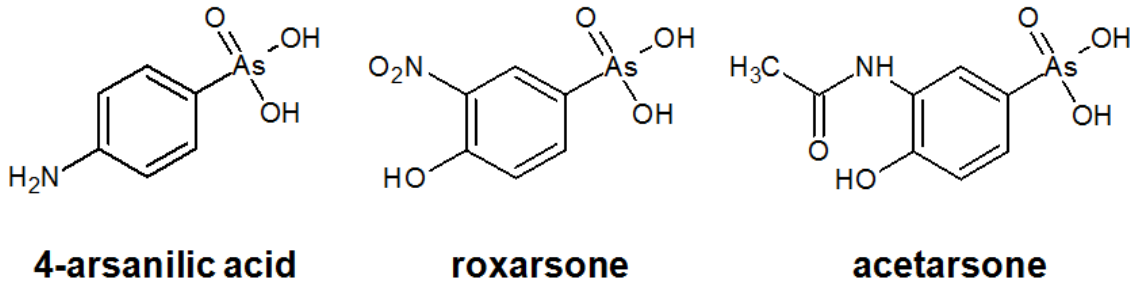

Figure 2.2. Molecular structure of 4-arsanilic acid, roxarsone and acetarsone.

Arsonic acid exhibits five Raman and SERS active modes in the 600-900 cm^{-1} range (figure 2.3-2.5). These modes can serve as a suitable marker to confirm the presence of organoarsenic agents in a sample. According to the conventional Raman spectrum for solid 4-arsanilic acid (Table 2.1), the symmetric and the asymmetric stretching bands for AsO_x occur at 792 cm^{-1} and 837 cm^{-1}, respectively; while the AsOH asymmetric stretching mode occurs at 727 cm^{-1}. Stretching modes assigned to As-C are observed around 592 cm^{-1} and 619 cm^{-1}. These five distinctive bands for the arsonic acid group are in good agreement with conventional Raman studies conducted by Cowen and collaborators with solid 4-arsanilic acid.[52]

Overlapping of As-C stretching modes in 4-arsanilic acid was observed under SERS conditions with an intense band centered at 596 cm^{-1}, while for roxarsone and acetarsone, the As-C bands are both shifted to higher wavenumbers (599 and 622 cm^{-1}, 622 and 645 cm^{-1}, respectively). Studies performed by Haresh[53] on the binding of $HAsO_4^{-2}$ to a silver surface identified three characteristic peaks at 792, 802 and 865 cm^{-1}, corresponding to ν_s As-O_{Ag}, ν_s and ν_{as} As-$O_{uncomplexed}$. These bands are the result of a weak monodentate binding of AsO_4^{-3} to the Ag surface.[53] A different result is observed at the Ag/PDMS surface where a single broad band around 792 cm^{-1} (780-800 cm^{-1}) occurs for all three arsenic species under study. This indicates that the As-O group of the drugs tends to bind more strongly onto the metal surface. As a result, the peak at 792 cm^{-1} combined with the characteristic fingerprint bands of these antimicrobials can be used as a marker to unequivocally identify the presence of arsenic antimicrobials in Ag/PDMS surfaces. The As-OH peak for 4-arsanilic acid appears as a shoulder at 737 cm^{-1} overlapped with the As-O_{Ag} broad band at 792 cm^{-1}. The formation of an Ag-O complex can be confirmed by examination of the 100-300 cm^{-1} region in SERS spectra of these antimicrobials, where a weak but broad Ag-O band occurs at 214 cm^{-1}. [53, 54] Alternatively, the intensity of this band as well as occurrence of in-plane and out-plane bending modes typical of the As-OH group varies between the drugs. These suggest that the drugs are binding at different orientations relative to the silver surface.

Table 2.1. 4-Arsanilic acid Raman and SERS spectra tentative band assignment.

Assignments	4-arsanilic acid (cm^{-1})		
	Normal Raman		SERS
	Lit*	Exp	Exp**
ν Ag-O		222	214[a]
16 a(a')			387
Out of plane COO def			509
ν As-C	605[b]	592	596
	636[b]	619	
4b(a'')			691
ν_s,ν_{as} As-OH	745[b]	727	737
ν_s AsO_x	810[b]	792	783
ν_{as} AsO_x	854[b]	837	828
ν_{as} AsO_2	913[a]		914
NH_2	980		984
18(a')			1006
7[a](a')		1081	1072
$\hat{a}_{as}$ C-H and $\hat{a}_{as}$ NH_2	1137		1131
9a(a')		1168	1168
3(a'), 14(a')			1238
19b(a')			1377
19b(b''), ν CC + δ CH			1443
19a(a')			1478
ν CC,		1587	1575
ν_s As=O, $As(OH)O_2^-$			1575

*** References: (a) Haresh et al.[53] (b) Cowen et al.[52]**

**** The vibrational modes were abbreviated as follows: ν_{as}: asymmetric stretching; ν_s: symmetric stretching; ν: stretching, δ: bending; ω: wagging; ip: in-plane and op: out-plane.**

2.6.2. Specific group frequencies of antimicrobials

2.6.2.1. 4-arsanilic acid

Raman and SERS spectra of 4-arsanilic acid $1x10^{-4}$ M are depicted in figure 2.3 and the assignment of relevant identification bands is presented in Table 2.1. The Raman spectra contain

the main characteristic arsonic bands that correspond to the group previously described and SERS spectra indicate the binding of the As-O with the silver surface of the substrate. Appearance of bands associated to the amino group in SERS spectrum, as well as its *para* orientation leads to the possibility that the orientation with respect to the silver surface of this molecule is flat. SERS spectrum collected for 4-arsanilic acid appears similar to the Raman spectrum concerning the modes corresponding to the arsonic group, whereas the intense band in SERS at 596 cm^{-1} corresponds to the overlap of the As-C stretching modes. A broad band at 783 cm^{-1} in the SERS spectra is attributed to AsO_x modes and overlapping of the As-OH band as a shoulder at 737 cm^{-1}, result of the red shift of the 727 cm^{-1} band. This red shift is associated with charge transfer from the molecule to the empty metal orbitals; the opposite effect leads to a blue shift.[7] It should be noted that the ν_s AsO_x is shifted from 792 to 783 cm^{-1} providing evidence of physical bonding with the silver surface. This argument can be sustained by the presence of a weak broad band at 214 cm^{-1} which is associated to the complex formation of AgO. Absence of bending modes of the As-OH at 1272 and 556 cm^{-1} as well as the absence of As-O[55] at 865 cm^{-1} within SERS spectra suggests the displacement of protons and the formation of a bidentate complex between the silver surface and AsO of the arsonic group.

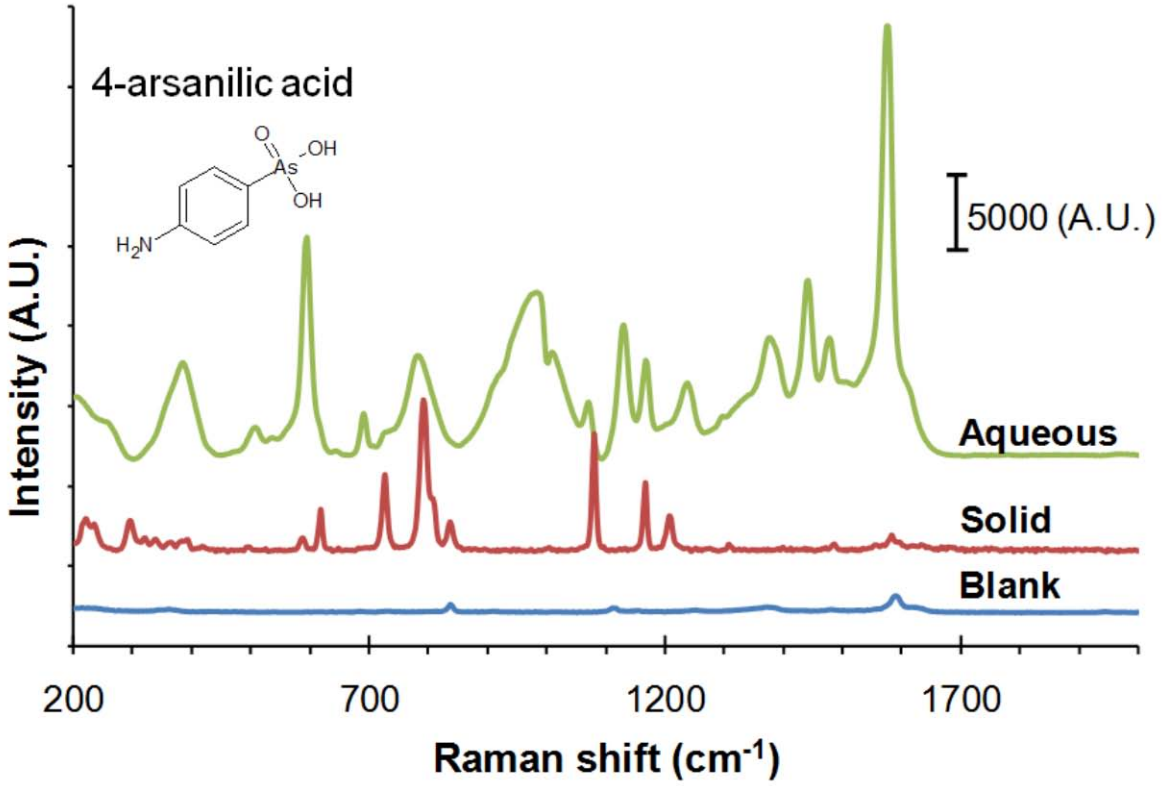

Figure 2.3. Raman spectra of 4-arsanilic acid taken after a 5 mW irradiation of the 632.8 nm excitation line of a He-Ne laser: Ag/PDMS water background (blank), conventional Raman of 4-arsanilic acid (solid) and SERS spectrum of 4-arsanilic acid ($1x10^{-4}$ M aqueous solution).

A very broad and intense band appears in SERS spectra centered at 984 cm^{-1}, enhancement of this band suggests overlapping of the signals associated to the arsonic group, such as As=O at 970 cm^{-1} and asymmetric stretch AsO_2 at 913 cm^{-1}; [53] as well as interaction of amino group with the silver surface. The spectroscopic data shows that there are at least three bands within this peak at 990 cm^{-1} and two shoulders around 920 and 1015 cm^{-1}. The interaction of the amino group with silver surface is demonstrated by the presence of a band at 1131 cm^{-1} which is characteristic of a NH_2 asymmetric bend.[56] Interaction of the amino group with the silver surface, as well as the physical adsorption of the arsonic group with the surface are supporting

evidence that the binding orientation of 4-arsanilic acid is flat with respect to the silver surface through these groups.

Aromatic ring vibrations such as in-plane bending vibration and aromatic ring vibrations[48] at 1168 and 1575 cm^{-1}, respectively, do not experience a significant shift in SERS spectra. Such small shifts are associated to weak intermolecular π bonding with the silver surface leading to physical adsorption.[49] Arsanilic acids exhibit acid base chemistries comparable to carboxylic acids. Nonetheless, the As atom tends to shift the asymmetric stretching modes of the As=O and $As(OH)O_2^-$ which occurs, respectively, as small shoulder overlapped to a strong band centered at 1575 cm^{-1}. Taking into consideration the interaction peak between the arsenic group and the amino group, as well as the weak interactions of the aromatic ring, the SERS spectra suggests that the orientation of the 4-arsanilic acid molecule is planar with respect to the silver surface. 4-arsanilic acid is structurally similar to 4-aminobenzoic acid, and therefore a similar sorptive behavior was expected. According to the spectroscopic data 4-aminobenzoic acids is adsorbed onto the silver in a planar orientation with respect to the silver surface.[56]

2.6.2.2. Roxarsone

The Raman spectra of roxarsone (figure 2.4) presents poor S/N ratio due to the strong background fluorescence of the drug. Roxarsone is characterized by analogous arsonic bands from 4-arsanilic acid. Raman bands at 619 cm^{-1} is assigned to As-C stretching, the band at 750 cm^{-1} is attributed to As-OH symmetric and asymmetric stretching and 809 cm^{-1} is due to AsO_x (see Table 2.2). The SERS spectrum is characterized by the broad band around 799 cm^{-1} which similarly to 4-arsanilic acid could indicate the formation of a complex between As-O and the

silver surface. Like in the case of 4-arsanilic acid the broadening and enhancement of this band indicates the binding of the drug onto the silver surface. The As-C stretching modes occur as intense broad bands at 599 and 622 cm^{-1}. Yet the appearance of a band at 553 cm^{-1} assigned to the As-OH out of plane bending[53] implies a monodentate binding rather than a bidentate binding onto the surface. Vibrational modes corresponding to the nitro group are also present in the Raman spectra at 1335 and 1517 cm^{-1} corresponding to the symmetric and asymmetric modes. In the SERS spectra of roxarsone, the nitro symmetric band is shifted from 1335 to 1323 cm^{-1}, indicating a binding through the oxygen atom.[48] Downshift and enhancement of the asymmetric modes of the nitro group are good indicators of this type of interaction.

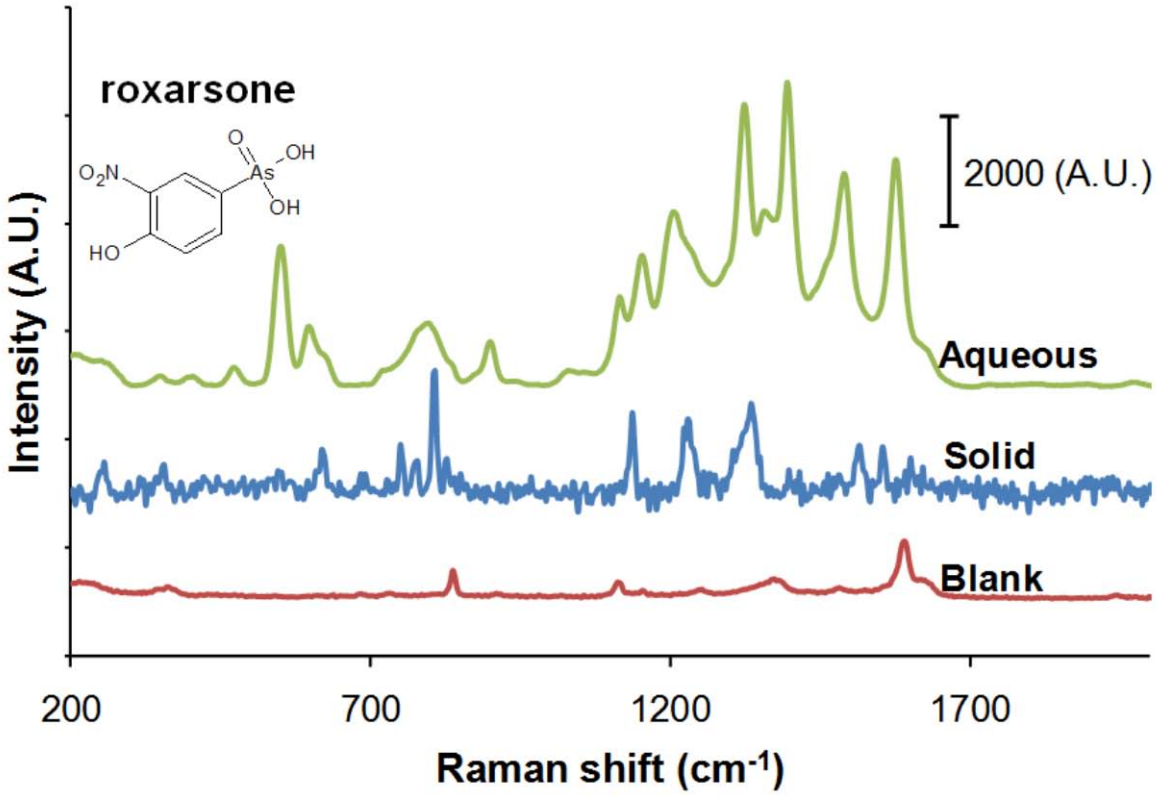

Figure 2.4. Raman spectra of roxarsone taken after a 5 mW irradiation of the 632.8 nm excitation line of a He-Ne laser: Ag/PDMS water background (blank), conventional Raman of roxarsone (solid) and SERS spectrum of roxarsone ($1x10^{-4}$ M).

The phenolic –OH rocking mode at 1229 cm^{-1} of the drug undergoes a minor shift and appears in SERS spectra as a shoulder of the band centered at 1205 cm^{-1}, thus suggesting a weak intermolecular interaction of the phenol group with the metal surface. Two Raman bands at 1555 and 1601 cm^{-1}, corresponding to the aromatic ring and NO_2 asymmetric stretching, are overlapped at 1575 cm^{-1} in SERS spectra and have contribution from the As=O and $As(OH)O_2^-$ bands. Presence of weak in-plane vibrations at 1031 cm^{-1} and aromatic ring vibrations at 404 and 472 cm^{-1} suggest a tilted sorption of roxarsone with respect to the metal surface. The interaction is mediated through binding of the arsonic and the nitro groups of the drug, and a rather weak interaction of the –OH group with the metal surface.

Table 2.2. Roxarsone Raman and SERS spectra tentative band assignment.

Assignments	Roxarsone (cm^{-1})			
	Normal Raman		SERS	
	Lit*	Exp	Lit*	Exp**
ν Ag-O			214[a]	215
		357		350
γ CC				404
ω CH				472
δop As-OH	556[a]			553
ν As-C				599
ν As-C	636[b]	619		622
ν_s,ν_{as} As-OH	745[b]	750		
ν AsOx	810[b]	809		799
ν_{as} AsO_2	913[a]			902
δip CH				1031
δ CH		1137		1115
ν CN				1152
OH def, ν C-O				1205
ρ OH	1223[d]	1232		1229
ν_s NO_2	1344[c]	1335	1326[c]	1323
ν CC, ν C-O				1356
ν CC		1398		1395
ν_{as} NO_2		1517		1490
ν CC		1555		1575
8a(a'), 8b(a'), ν_{as} NO_2		1600		1575
ν_s As=O, $As(OH)O_2^-$				1575

*** References: (a) Haresh et al.[53] (b) Cowen et al.[52] (c) Raj. et al.[48] (d) Fleger et al.[49]**

**** The vibrational modes were abbreviated as follows: ν_{as}: asymmetric stretching; ν_s: symmetric stretching; ν: stretching, δ: bending; ω: wagging; ip: in-plane and op: out-plane.**

2.6.2.3. Acetarsone

Raman and SERS spectra of acetarsone also illustrate the characteristic arsonic bands within the 600-900 cm^{-1} region (figure 2.5). Its Raman spectrum has two bands at 756 and 802 cm^{-1} assigned to As-OH and AsO_x vibrational modes for acetarsone (see Table 2.3). Similarly to roxarsone, the SERS spectrum shows a strong band at 792 cm^{-1} attributed to the As-O interaction between the O and the Ag surface. The formation of this complex is supported by presence of an intense band at 215 cm^{-1} assigned to AgO. The out-plane and in-plane bending modes for AsOH occurs at 556 and 1269 cm^{-1} indicating the presence of As(OH) at the metal surface. The absence of band at 865 cm^{-1} corresponding to $AsO_{uncomplexed}$ suggests the formation of a monodentate complex as with roxarsone. In conventional Raman, the stretching modes for As-C occur at 609 and 649 cm^{-1} whereas under SERS conditions they appear overlapped centered at 622 cm^{-1} with a small shoulder at 645 cm^{-1}. The characteristic bands of the amido and phenol group allow unequivocal characterization of this molecule. Bending modes for the nitrogen from the amido group appear in the SERS spectra at 1575 cm^{-1} while the 1455 cm^{-1} band corresponds to the CH bend of the methyl group. These two bands along with NH and CH bending band at 949 cm^{-1}. They are not significantly shifted from its normal Raman position (952 cm^{-1}) indicating a weak interaction between the NH and CH_3 of the amido group and the metal surface. Absence of the C=O stretching mode at 1650 cm^{-1} in accordance with previous studies is another indicator of a weak binding of the drug to the metal surface.[57, 58]

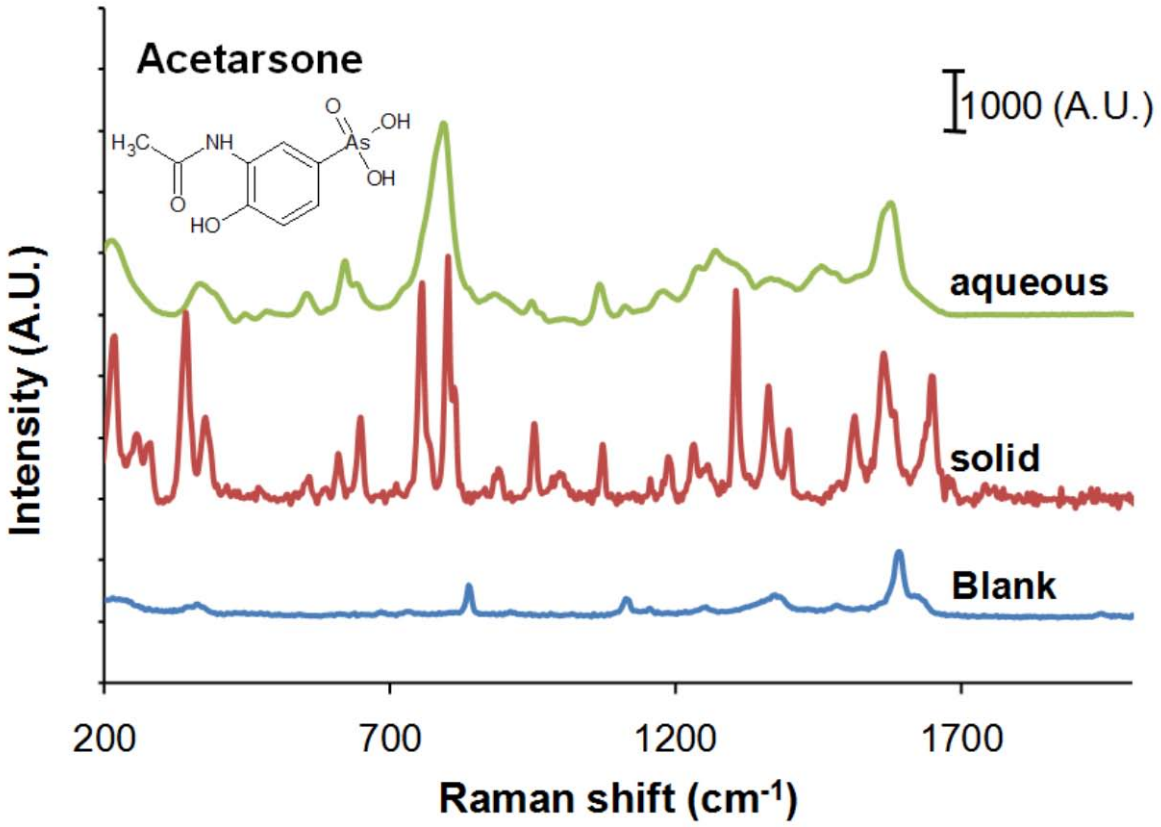

Figure 2.5. Raman spectra of acetarsone taken after a 5 mW irradiation of the 632.8 nm excitation line of a He-Ne laser: Ag/PDMS water background (blank), conventional Raman of acetarsone (solid) and SERS spectrum of acetarsone (1x10^{-4} M).

Ring stretching modes at 1569 cm^{-1} are overlapped with the nitrogen band at 1575 cm^{-1}, although no significant shift is noted suggesting a tilted orientation of the ring. This is supported by presence of out of plane CH bending mode at 882 cm^{-1}. The molecular orientation proposed for acetarsone with respect to the silver surface is tilted with a weak interaction through the nitrogen and methyl group of the acetamido group as well as a monodentate complex between the arsenic acid group and the silver surface.

Table 2.3. Acetarsone Raman and SERS spectra tentative band assignment.

Assignments	Acetarsone (cm^{-1})			
	Normal Raman		SERS	
	Lit*	Exp	Lit*	Exp**
ν Ag-O			214[a]	215
16a(a')		377		370
Out of plane ring def				445
Ring Breathing, ν C-OH, ν C-				486
δop As-OH	556[a]	559		556
ν As-C	605[b]	609		622
	636[b]	649		645
ν_s,ν_{as} As-OH	745[b]	756		792
ν AsO_x	810[b]	802		792
δop CH		889	860[c]	882
δ NH, δ CH	962[c]	952		949
ν C-O		1072		1066
δ CH				1112
		1186		1180
δ CH, δ NH , ν CO	1232[c]	1235	1240[c]	1236
δip As-OH	1272[a]			1269
δ CN, δ OH, δ C=O		1362		1365
δ CH methyl	1440[c]		1453[c]	1455
ν CC,δ C-O, δ N-H, As=O	1557[c]	1563		1569
δ NH			1582[d]	1575
ν_s As=O, $As(OH)O_2^-$				1575
ν C=O	1652[d]	1650		

* References: (a) Haresh et al., [53] (b) Cowen et al.,[52] (c) Smith et al.,[57] (d) Y. Wang et al. [58]
** The vibrational modes were abbreviated as follows: ν_{as}: asymmetric stretching; $\nu_{s:}$ symmetric stretching; $\nu_{:}$ stretching, δ: bending; ω: wagging; ip: in-plane and op: out-plane.

CHAPTER 3

DESIGN AND CHARACTERIZATION OF HYBRID MORPHOLOGY NANOARRAYS AS PLASMONIC RAMAN PROBES FOR ANTIMICROBIAL DETECTION

This chapter is a revised version of an article under the same name published in Applied Spectroscopy by Jenifier Olavarría-Fullerton, Raymond A. Vélez, Sabrina Wells, Michael J. Sepaniak, Samuel P. Hernández-Rivera and Marco A. De Jesús.

Olavarría-Fullerton, J.; Vélez R.A.; Wells S.; Sepaniak M.J.; Hernández S.P.; De Jesús, M.A. Design and characterization of hybrid morphology nanoarrays as plasmonic Raman probes for antimicrobial detection. *Appl. Spectrosc.* **2013**, *67(11)*, pp 1315-1322.

The use of "we" in this chapter refers to my co-authors and me. My primary contributions to this article included: (A) design of the project and development of experimental protocols to validate nanolithographic arrays, (B) design and fabrication of hybrid nanoarrays, (C) collection and interpretation of most of the analytical data, (D) collection and interpretation of cited data, and (E) most of the article write up.

3.1. Introduction

Since investigators such as Fleishman, Hendra, and McQuillan;[6] Jeanmaire and Van Duyne;[14] and Albrecht and Creighton[15] observed the surface enhanced Raman scattering (SERS) effect, the phenomenon has been prone to lack of proper signal reproducibility mostly due to the inability to create a nanostructured surface with uniform plasmonic responses.[6,19] As a result, considerable strives has been made in the search for highly reproducible SERS active surfaces capable of fast and reliable ultra-trace detection of target analytes. This evolutionary journey progressed SERS substrate technology from electrochemically roughened electrodes[6] and colloidal suspensions[43,59] to highly sophisticated nanolithographic structures with improved

control of the morphology as well as its plasmonic response.[26,29,60,61] Nanolithography is a cutting-edge fabrication approach that open new opportunities to accurately adjust the shape, size, and inter-particle distribution of the nanostructured features on the surface to optimize its SERS responses within the visible region of the electromagnetic spectrum.[19,62]

Of all the various nanolithographic methods, electron beam lithography (EBL) has lead to the construction of diverse SERS-active substrates with unique characteristics. Moreover, the combination EBL liftoff protocols and reactive ion etching (RIE) have proven effective on the fabrication of robust, more durable, periodic plasmonic nanoarrays.[17,25] To this date, the majority of the EBL and RIE work has been focused on the construction of extended nano-arrays of a single geometrical pattern and morphology, such as diffraction gratings with simple ridges and grooves,[17,25] or more complex diffraction pillars.[18,24] Despite the improved SERS performance attained with these gratings, its uniform morphologies lead to complex diffraction patterns. These patterns result in resonant modes whose wavelength positions and field enhancements are limited to well defined dipolar modes.[63]

Our team of researchers has been using EBL methods to improve substrate performance for over a decade, ranging from simple metal-polymer nano-arrays to aggregates that mimic the randomness of colloidal nanoparticles.[28,29,30] The work presented here uses hybrid-pattern nano-arrays as a general purpose substrate that will result in enhanced SERS performance at multiple wavelengths. Since plasmonic excitations are strongly dependent on surface morphology,[62] the hybridization of two different geometrical features could create a versatile substrate that may be tuned for multiple wavelengths. Although this approach may compromise performance, it is an acceptable trade-off when considering broadening the excitation wavelength capabilities. The

use of geometrical features with enlarged surface areas could provide higher loading capacity thus enabling its viability for quantitative applications. The developed nanostructures allowed the unequivocal identification of trace 4-arsanilic acid in aqueous media by SERS. The impact of nanoparticle orientation and inter-particle spacing on SERS enhancement factors will be discussed. The protocol is presented for the successful fabrication of hybrid nanostructured substrates with extended areas of accurate replication that permits finite-domain time-difference (FDTD) analysis to corroborate the plasmonic performance of the nanostructured substrates.

3.2. SERS substrate preparation

3.2.1. Fabrication of Silicon Dioxide/Silicon substrates

The EBL master patterns were designed with AutoCAD® 2005. The nano-arrays were characterized as 50 × 50 μm arrays of hexagons and ellipses with varied particle spacing (100 nm - 300 nm) and orientation. As shown in Table 3.1, the dimensions of the ellipses were 200:100 nm (longitudinal axis: transversal axis) and the hexagons were 200:100 nm (length between two opposite corners, individual face). Two particle orientation designs were investigated: ellipses parallel to the hexagons (PEH) and ellipses orthogonal to the hexagons (OEH); both with variable interparticle spacing (from 100 nm to 300 nm).

Table 3.1. AutoCAD® design properties for the pattern nanofabrication.

Pattern/ Acronym	Shape	Dimensions (nm)		View	Illustration
		Length (L) x Width (W) x Height (H)	Gap*		
Parallel Ellipse Hexagon PEH*G	Hexagons	200 x 100 x 250	100	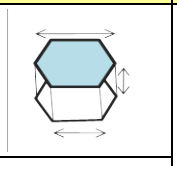	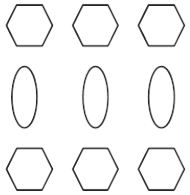
			150		
			200		
			300		
	Ellipses	200 x 100 x 250	100	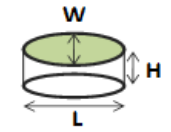	
			150		
			200		
			300		
Orthogonal Ellipse Hexagon OEH*G	Hexagons	200 x 100 x 250	100	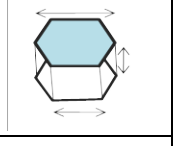	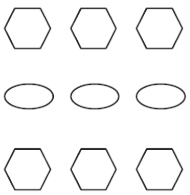
			150		
			200		
			300		
	Ellipses	200 x 100 x 250	100	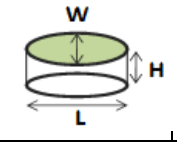	
			150		
			200		
			300		

The substrates were fabricated according to the liftoff pillar method previously described by Wells et al.[28] In general, a 2 inch silicon wafer was initially baked for 45 min at 250 ^{o}C (Figure 3.1). Then, a film of positive resist ZEP 520 A was spin-coated onto the wafer for 45 s at 6000 rpm and subsequently baked at 180^{o} C for 2 min. The final thickness of the resist was estimated to be 300 nm (based on the manufacturer's guidelines[64]).

The wafer was placed under vacuum in a JEOL JBX- 9300 Field Emission 100 kV e-beam for pattern lithography onto the resist-coated wafers using a dose of 420 μC/m^2. Once exposed, the wafer was developed in xylenes for 30 s, followed by an isopropyl alcohol (IPA) rinse. In order to obtain more defined pillar sidewalls, the wafer was exposed to O_2 for 6 s at 100 W with a Technics Reactive Ion Etching System. This step was followed by a chrome

deposition performed by an electron-beam dual gun evaporation chamber (Thermonics Laboratory VE-240) at a rate of 1.0 Å/s until reaching a final thickness of 10.4 nm. A liftoff procedure (3 minutes in acetone, 2 minutes in isopropyl alcohol (IPA), and deionized water (DIW) rinse) was used to remove the remaining resist while leaving the Cr mask on the Si wafer. Si pillars were obtained by a shallow etching process, which consists of exposing the wafer to a mixture of argon, SF_6 and C_4F_8 with an Oxford RIE resulting in a nominal height of 250 nm. The wafer was then placed in a chrome photo-mask etchant (Cr-14S) for 15 minutes to remove the Cr from the pillar tops. Finally, a 20 nm layer of silicon dioxide (SiO_2) was deposited on the wafer employing an Oxford Plasma Enhanced Chemical Vapor Deposition system at a rate of 1.2 nm/s.

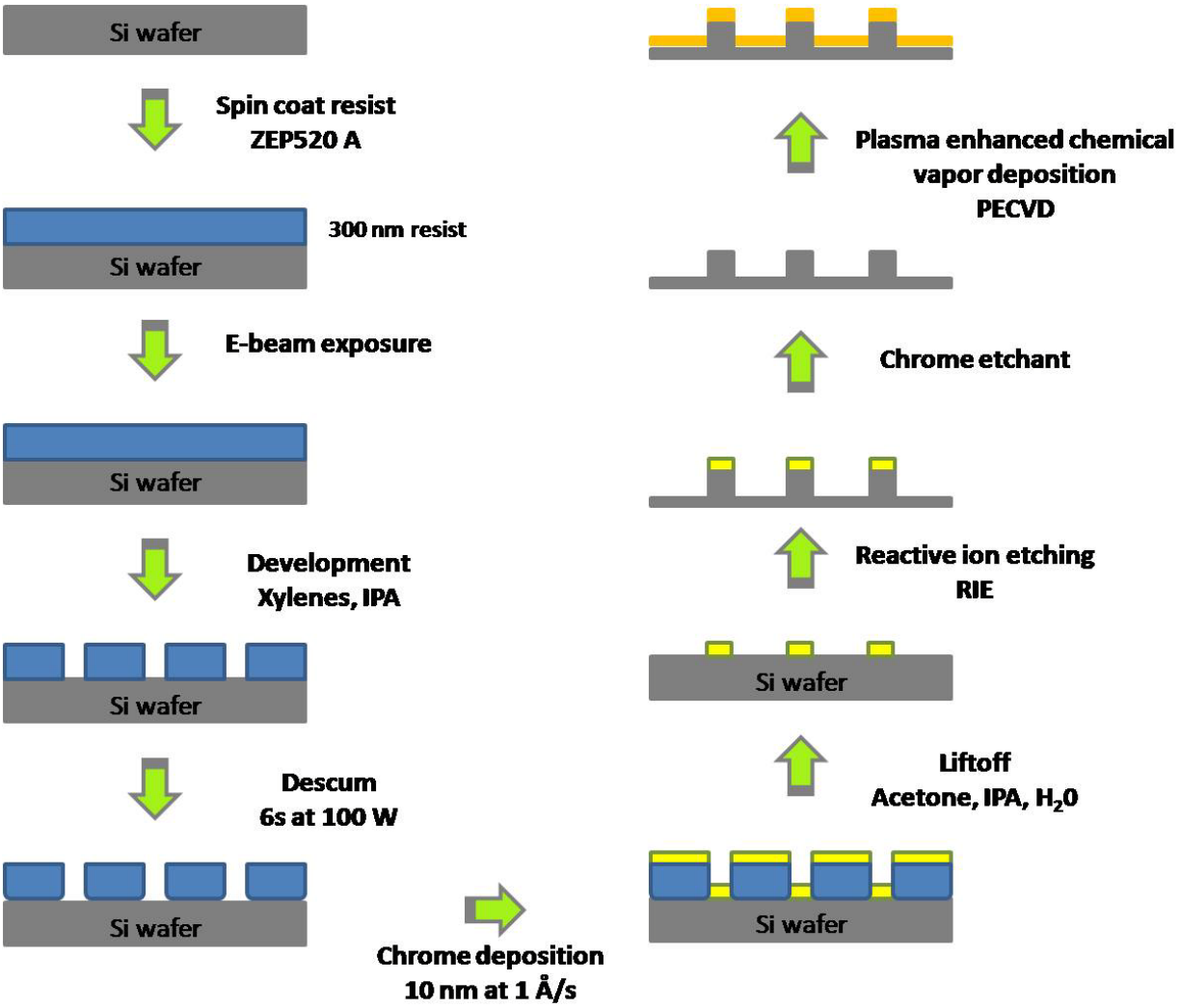

Figure 3.1. Diagram of the liftoff pillar method for the fabrication of the SiO_2/Si substrates

3.2.2. Substrate deposition parameters

SiO_2/Si substrates were metalized under vacuum (1.0 (± 0.2) × 10^{-6} torr), in an electrothermal evaporator (Edwards Auto 306 Evaporation System, or its equivalent). The thickness of the metal coating was registered by a quartz analytical microbalance integrated on the system. The evaporation was performed with standard Ag shots (99.9999%, ACROS) at a rate of approximately 1.5 (± 0.1) Å/s. Thickness of the SERS active surface was in the range of 25 (± 2)

nm. After deposition, all substrates were placed under vacuum and in dark conditions until required for analysis. Polydimethylsiloxane (PDMS) nanocomposites were prepared and metalized as described in previous work.[21]

3.3. Sample preparation

The reagent 4-Arsanilic acid (99%) was purchased (Acros Organics) and a stock of 1 mM 4-arsanilic acid was prepared with 18 mΩ deionized water (DIW, Barnstead, Co.). The laboratory sample used for SERS studies was a 50 µL aliquot of a 1.0×10^{-4} M 4-arsanilic acid. The reagent 4-aminobenzenethiol (4-ABT) was purchased (Aldrich) and an aliquot of a 1×10^{-3} M 4-ABT stock solution was diluted in sufficient ethanol to produce a 1×10^{-5} M solution; this was employed as a probe molecule for surface-enhancement factor (SEF) calculations.

3.4. Instrumentation, data acquisition and analysis

SERS spectra for the arsenic drug were acquired in a LabRam-HR Microscope from JY-Horiba. The instrument uses a 50x Nikon objective that delivers an effective laser power of 2.5 mW of the 633 nm line of a HeNe Laser over the sample. Detection of arsenic compounds took place by carefully placing substrates in a flow cell. Once centered, the cell was filled with the analyte solution. The array was then focused and the XY translational mechanical stage was programmed to scan in 5 micron steps from -35 µm to 35 µm in XY direction, taking one acquisition of 1 s at each point. Resulting SERS spectra for 4-arsanilic acid 1×10^{-4} M from mapping over the $Ag/SiO_2/Si$ nanoarrays were used to calculate the average peak area of the As-C stretching band at 594 cm^{-1}.

A Renishaw Raman Spectrometer RM 2000 equipped with a Leica microscope was employed to acquire SERS spectra of 4-ABT. The instrument uses a 50x Olympus objective that delivers 2.85 mW and 2.53 mW of the 532 and 785 nm line from a diode laser, respectively. A HeNe laser that delivers 3.32 mW of the 633 nm line employing the 50x objective was used. To collect the SERS spectra of 4-ABT for surface enhancement factor (SEF) calculations, the $Ag/SiO_2/Si$ substrates were first immersed for 60 seconds in a 1×10^{-5} M solution of 4-ABT. The substrates were then dipped into DIW. The characteristic stretching carbon-sulfur (C-S) Raman vibrational mode of 4-ABT at 1078 cm^{-1} in SERS spectra was used to evaluate the SEF. Neat solid Raman spectra were acquired in a capillary tube, where the same vibrational mode for 4-ABT at 1088 cm^{-1} was used for SEF calculation.

3.5. Safety considerations

Special care must be taken when handling arsenic compounds since they are carcinogens, and potentially toxic via inhalation, ingestion and skin contact. Appropriate safety equipment, such as chemical safety goggles, nitrile gloves and lab-coat must be used at all times while handling these compounds, as well as, adequate ventilation. Wastes must be disposed of properly and in accordance with hazardous waste regulations.

3.6. FDTD Simulations

The Lumerical® FDTD Solutions software articulates Finite-Difference Time-Domain (FDTD) to effectively solve Maxwell's equations required to model the electromagnetic fields (EMF) induced by the propagation of light across the substrate based on its physical properties (i.e. dimensions, material dielectrics).[65] A simple 3D model of the array's unit cell (a hexagon

and an ellipse arranged in a parallel form) was comprised within a 2 nm^2 mesh simulation region. Boundary conditions consisted of (1) periodic along xy axis and (2) perfectly-matched layers (PML) at the z axis. A plane-wave source (5 nm from top of Ag layer surface and parallel to the transversal axis to the nanoarray) was used to simulate an incident laser (λ = 500 nm to 850 nm) with various monitors strategically placed to obtain EMF data. Two additional systems consisting of either ellipses or hexagons were modeled besides the fabricated PEH substrate using the aforementioned conditions for assessment of PEH simulated performance.

3.7. Results and discussion

The advantages of nanofabrication were exploited toward the design and construction of a hybrid nanoarray substrate over extended areas with increased reproducibility and contrast. Performance of the EBL/RIE procedure was first assessed by collecting the 1.50 kV micrographs of the nanoarrays (figure 3.2). According to these micrographs, the nano-lithographic process resulted in pillars well within the projected specifications of less than 10% and 15% difference in its coefficient of variation (CV) for both, dimensions and inter-particle gap, respectively. The final step of the fabrication process consisted of depositing a thin film of SiO_2 since studies have shown that it exhibits superior dielectric and plasmonic properties than Si for SERS applications.[66]

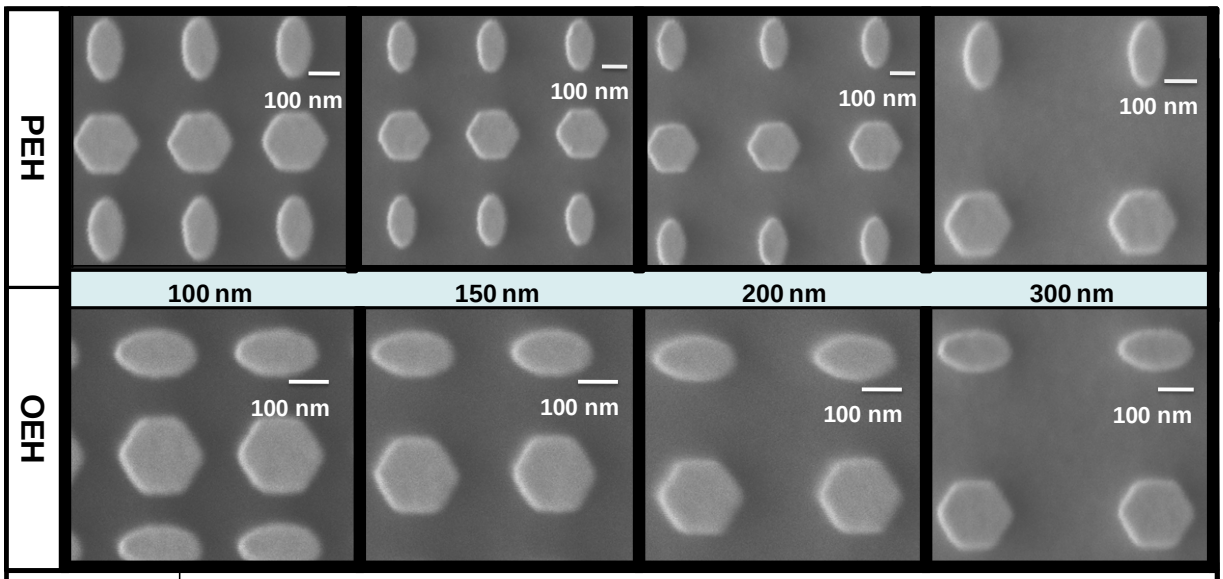

Interparticle spacing	Nanoarrays							
	PEH				OEH			
Expected gap, nm	100	150	200	300	100	150	200	300
Resulting gap, nm	85 (±12)	143 (±7)	201 (±15)	298 (±11)	80 (±7)	136(±8)	183 (±8)	293(±10)

Figure 3.2. SEM micrographs of EBL fabricated PEH (top) and OEH (bottom) substrates with average interparticle spacing ranging from 100 – 300 nm following deep RIE.

3.7.1. SERS detection

The EBL fabricated nano-arrays were assessed for SERS detection of arsenic drugs employing 4-arsanilic acid as a probe analyte. SERS spectra collected for the nano-arrays, illustrated in figure 3, resulted in the characteristic vibrational modes for this compound and were consistent with those previously reported.[21] Bands associated to the arsonic group are identified within the 600-900 cm^{-1} region. The Ag/PDMS nanocomposites resulted in poorly resolved responses in the 592 cm^{-1} region that is attributed to the As-C symmetric and asymmetric stretching modes. Use of the newly nanofabricated substrates allows for an improvement in both signal response and resolution, thus enabling a more pristine differentiation

of these modes (592 and 619 cm^{-1}) consistent with the neat Raman spectra (reported elsewhere).[21] An intense AsO_x mode with an As-OH stretching as a shoulder is also observed at 795 cm^{-1}. Another characteristic band associated with the arsonic group as well as the interaction of the amino group with the metallic surface is present at 993 cm^{-1}; while the vibrational NH_2 asymmetric bend is observed at 1137 cm^{-1}.

The plasmonic performance of the constructed nano-arrays was compared to silver polydimethylsiloxane (Ag/PDMS) nanocomposites. In our research, Ag/PDMS substrates have proven a highly efficient and reliable substrate with superior SERS responses to traditional SERS substrates. We commonly use it as a reference material to test if the newly developed substrates exceed its performance. Figure 3.3 illustrates SERS spectra of 4-arsanilic acid (1×10^{-4} M) acquired with the PEH nano-array of 200 nm interparticle spacing and the Ag/PDMS substrate. SERS vibrational modes of 4-arsanilic acid, such as stretching As-C and As-O modes as well as NH_2 modes, appear to be considerably enhanced when employing the nano-array providing SERS signal intensity within one order of magnitude over the signal resulting from Ag/PDMS. This is the result of differences in surface morphologies among the employed materials that directly affect their field enhancements. The fine control and definition of nanoscale features achieved by EBL/RIE provides improved excitation of the plasmonic response, contrary to the polymeric nanostructures where the random (fractal-like) distribution of the embedded metal nanoparticles limits the effectiveness of its field enhancement.[45] The SERS data for 4-arsanilic acid was collected with 532, 633 and 785 nm excitation wavelengths and normalized according to laser power and acquisition time. However, the collected spectra at 532 and 785 nm resulted in low band intensities relative to that at 633 nm wavelength.

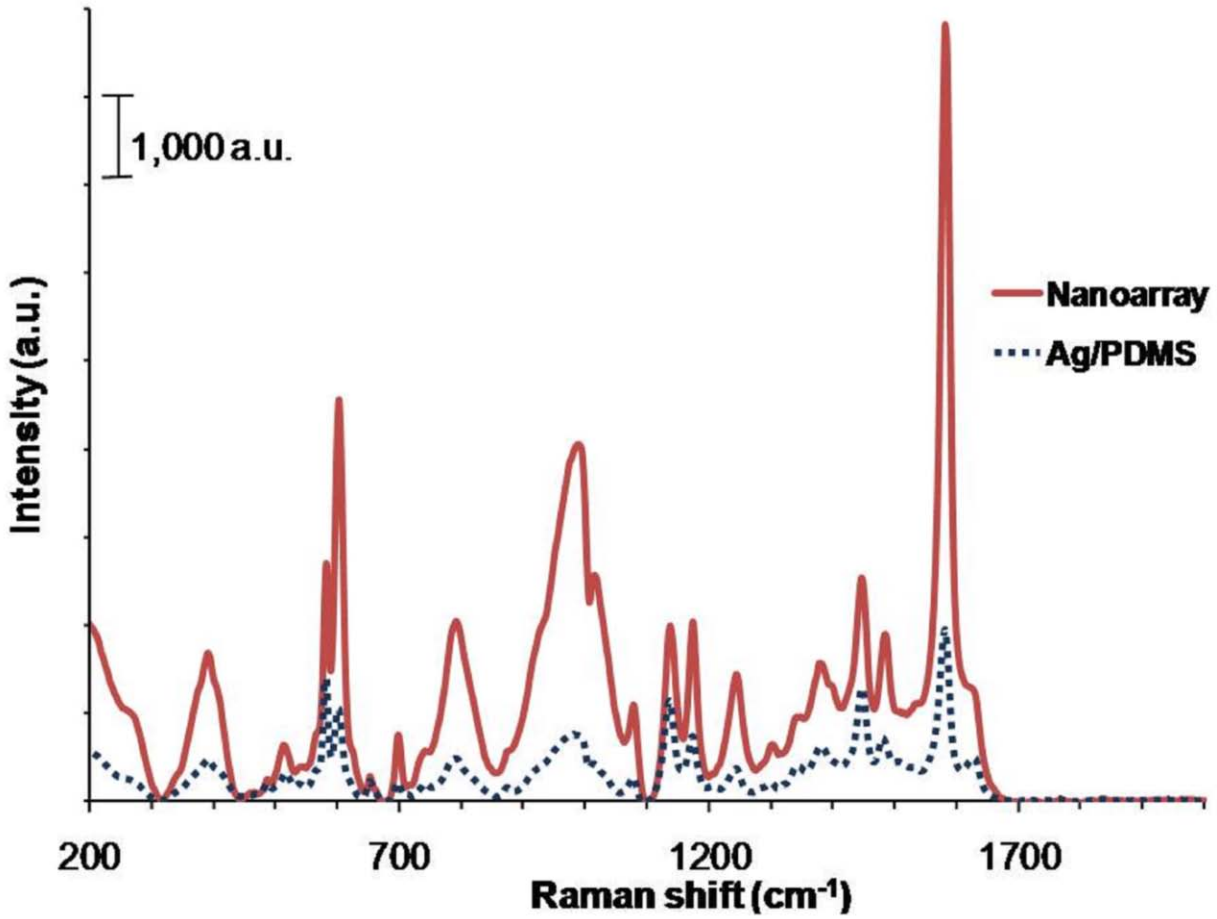

Figure 3.3. Comparison of average SERS spectra of 4-arsanilic acid (1 x 10^{-4} M) using PEH nanoarrays with 200 nm gap and Ag/PDMS nanocomposites after 2.5 mW irradiation of a 633 nm excitation line of a HeNe laser.

3.7.2. Nanoparticle orientation effect

Particle orientation is one of the main optimization parameters. The frequency and magnitude of the maximum field enhancement depends strongly on particle orientation.[19] The nano-arrays fabricated consisted of patterning ellipses and hexagons where two particle orientations were explored. The first consisted in arranging the ellipses parallel to the hexagon (PEH) and the other of ellipses oriented orthogonal to the hexagons (OEH). Since the ellipse is the most polarizable feature it is expected to play a primary role in the plasmonic properties of

the surface over the hexagon. Therefore, the PEH arrays, which have the longitudinal axis parallel to the polarization vector, are expected to provide improved SERS signal enhancement over the OEH arrays where the transversal axis is parallel to the polarization vector. In order to determine the performance of these arrays, the SERS spectra for 4-arsanilic acid (1×10^{-4} M) were collected employing both substrate orientations. The peak area for As-C stretching mode at 594 cm^{-1} was monitored for comparison (presented in figure 3.4). This figure illustrates that all the PEH substrates result in a stronger signal enhancement for the selected vibrational mode than do the OEH substrates. It is noted that for even the best performing OEH substrate, with a 300 nm gap, its enhancement is well below the signal resulting from the worse-performing PEH array. This behavior is in accordance with our expectations since, as mentioned above, the PEH nano-arrays have the longest axis of the ellipse aligned with the laser polarization, and according to electromagnetic mechanism, this is where more intense scattering is observed since it is the most polarizable direction.[8] Since the shortest axis of the ellipses of nanoarrays with orthogonal orientation is parallel to the laser polarization, poor SERS signal enhancement was anticipated.

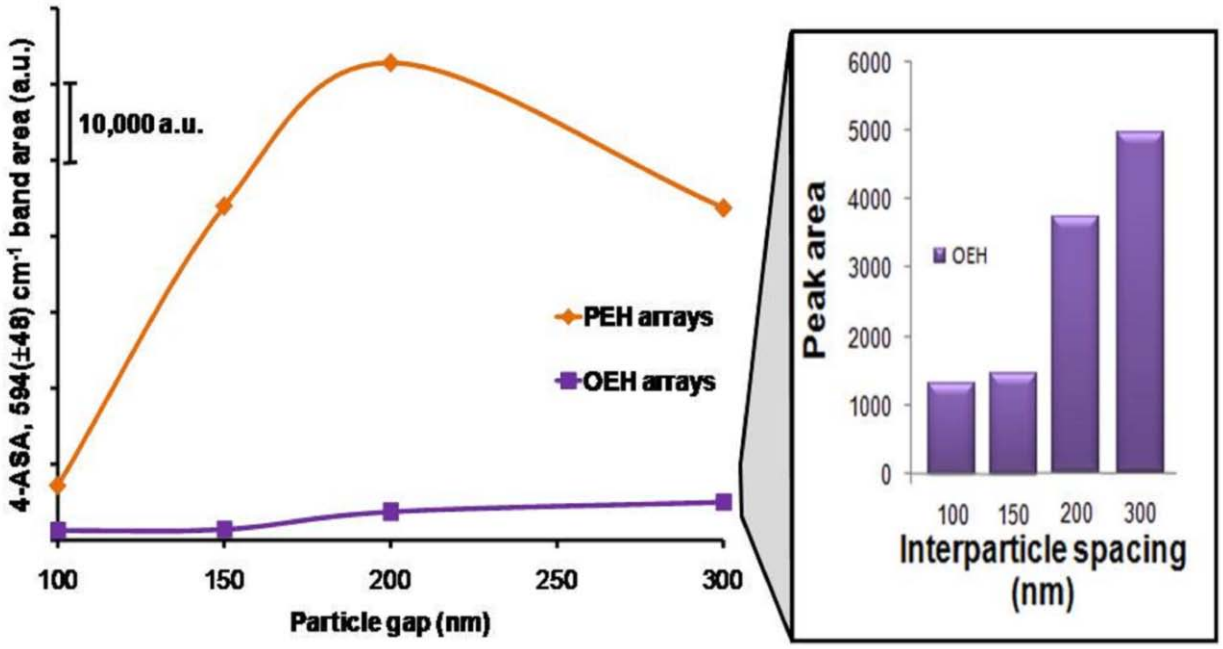

Figure 3.4. Nanofabricated array response for As-C stretching mode at 594(±48) cm^{-1} accounting for interparticle spacing and orientation after irradiation with 2.5 mW of a 633 nm excitation line of a He-Ne laser.

3.7.3. Interparticle spacing effect

Nano-arrays employed in this study had an interparticle spacing ranging from 100 - 300 nm whereas each pattern array, that is PEH and OEH, rendered different behavior in SERS signal enhancement. The graph in figure 3.4 illustrates the relationship between the peak area for As-C stretching band and interparticle spacing of both nanofabricated substrates. It is noted that for PEH arrays, the SERS band area increases with gap size, reaching a maximum at 200 nm, and then decreases, thus indicating that the 200 nm interparticle spacing resulted in superior SERS enhancement for this array. The bar graph within Figure 4 illustrates that for the OEH substrate, the interparticle spacing at 100 and 150 nm renders essentially the same SERS band area, with an increase of ~2.5-fold increase for 200 nm, and an additional increase at 300 nm.

3.7.4. Finite-difference time domain (FDTD) simulations

A qualitative perspective of the expected signal intensities for the PEH nano-arrays is observed in Figure 3.5a. The $|E|^2$ vs. λ curve for the hexagon depicts a well-defined band with a maxima at λ = 543 nm and two unresolved bands at 634 nm and 734 nm for the hexagon. The ellipse shows one strong band at 536 nm with a maximum intensity of 1341 a.u. The signal decreased to about 200 a.u. at 625 nm and remained consistent until 800 nm where the signal reaches insignificant levels of detection. The FDTD data predicts a suitable response for target Raman lasers with wavelengths of 633 nm and 785 nm (due to the hexagon feature of the PEH nano-arrays) whereas the maximum performance is expected at 532 nm (for the ellipse).

The simulated performance of infinite arrays consisting of either hexagons or ellipses was compared to the PEH system (Figure 3.5b). The hexagon substrate depicts three bands as in the PEH but with slight differences in the wavelength of the maxima. For instance, a blue shift is observed for the band at 551 nm in the hexagon substrate to 543 nm in the PEH. This shift is also accompanied by a 64% increase in signal intensity for the PEH substrate in this particular wavelength region. A blue shift is also observed for the second PEH band at 634 nm to 604 nm in the hexagon with a signal decrease from 360 a.u. to 215 a.u.; which constitutes a 40% signal drop. On the contrary, the third PEH band at 780 nm was slightly shifted to 796 nm but with a 49% signal increase. This simulation data reveal enhanced performance for the hexagon feature when combined with the ellipse in the PEH arrays.

Improvement in the ellipse plasmonic signal is also observed when located in the PEH system in contrast to the single feature (Figure 5b). The ellipse substrate depicts band maxima of 1134 a.u. at 521 nm which undergoes a red shift to 536 nm, with an 18% signal increase.

However, the most significant enhancement was the signal increase observed at 780 nm of 0.9 a.u. in the ellipse substrate to 71 a.u. when in the PEH system. This is the result of the red shift of the band from 720 nm (ellipse only) to 734 nm (PEH-related ellipse). The PEH system not only resulted in plasmonic signal increases for the ellipse but, most importantly, induced a response for the target 785 nm Raman laser region that was not attainable if using the ellipse feature only.

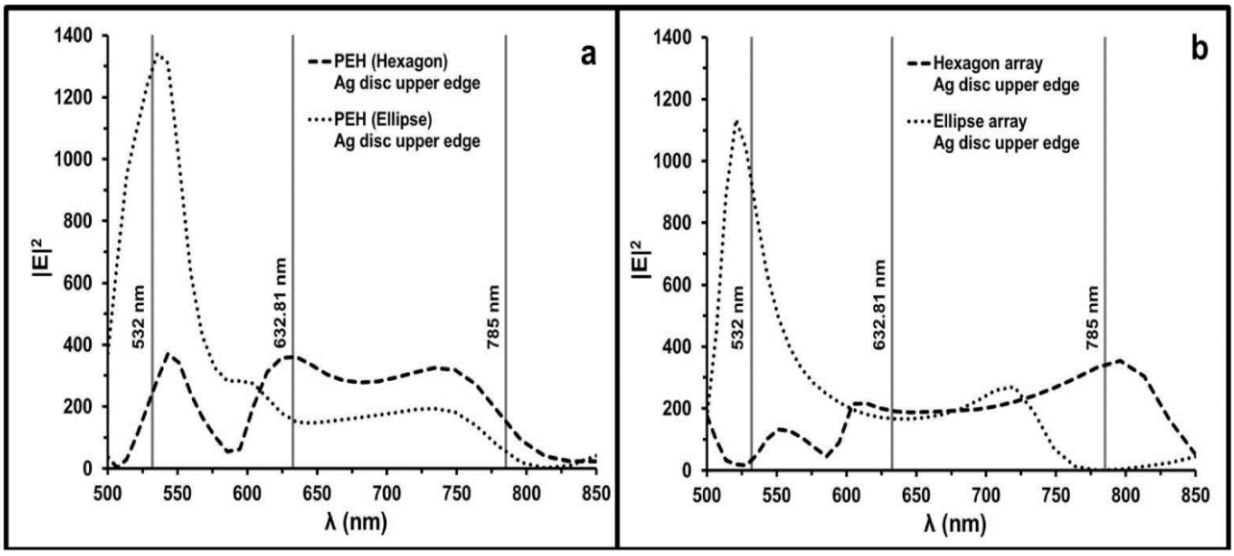

Figure 3.5. FDTD data depicting $|E|^2$ as a function of wavelength for: (a) hybrid PEH nanoarrays profile (b) individual pattern profile. The incident wavelengths used during the experimental procedures (λ= 532 nm, 633nm, and 785 nm) are identified.

A clearer representation can be observed with the $|E|^2$ distribution across the x-axis (Figure 3.6a). The wavelengths are not exactly the same to those used for the experiments due to the amount of frequency points programmed for the simulation. However, these simulated wavelengths (528 nm, 635 nm, and 780 nm) are not expected to portray significantly different $|E|^2$ trends from the raw signal from the experimental spectra (532 nm, 633 nm, and 785 nm) due to the proximities between the theoretical and experimental incident wavelengths. As noticed

before, the hexagon signal intensities are expected to remain somewhat constant across all three wavelengths and the ellipse should produce an inherently stronger plasmonic signal at 532 nm. The PEH array is expected to provide near-equivalent intensities for the hexagon and ellipse at 633 nm. This suggests that current hexagon dimensions characterize it as a robust feature for SERS detection, in contrast to the ellipse as directed towards lower wavelengths for a more effective plasmonic signal. A graphical depiction of the $|E|^2$ distribution ($\log_{10}$ scale) along the xy and xz planes for the simulation wavelengths 528 nm, 635 nm, and 780 nm can be appreciated in Figure 3.6b. Once again, the upper Ag edges show a strong signal on the same order as the previously discussed behavior (the ellipse shows a red shift, the hexagon is somewhat consistent, and λ value near the 633 nm region gives similar intensities on both elements). Simulations correlate to experimental data, where the apparent SERS signal for the 4-ABT C-S stretching mode at 532, 633 and 785 nm resulted in band areas of 234, 15 and 13 A/mW*s respectively for the PEH unit cell. The apparent signal trend is the result of the combined effect of the electrochemical, chemical and surface area effects on the signal enhancement. This substantiates that the PEH system produces a greater signal response for shorter wavelengths (520 nm, 532 nm) than for the longer wavelengths (780 nm, 785 nm), as with the normalized signal.

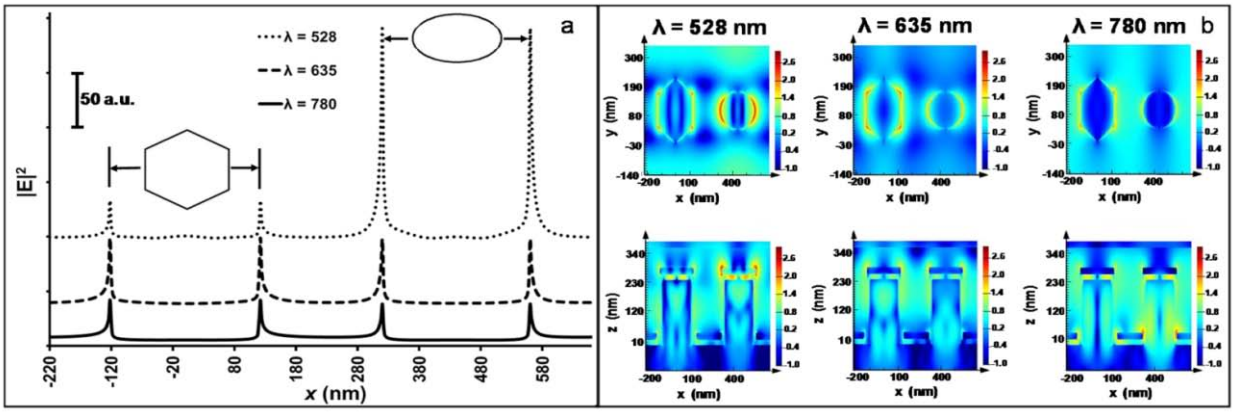

Figure 3.6. $|E|^2$ distribution across the FDTD polarization axis (x, nm) at variable simulated wavelengths (a). The $|E|^2$ maxima observed with peaks at x = -122 nm and 122 nm correspond to the hexagon, whereas peaks at 320 nm and 560 nm are of the ellipse. The geometric figures are only a graphical representation (these are not to scale with the *x*-axis). (b) Simulated $|E|^2$ distribution (log_{10} scale) on the xy plane (top row) and xz plane (bottom row) for λ = 528 nm, 635 nm, and 780 nm. The scale bar is normalized from -1 to 3.

3.7.5. Surface enhancement factor (SEF)

The most commonly used equation to assess SERS enhancement factors across different substrates is given by:[13]

$$SEF = \frac{I_{surf}}{I_{vol}} \; x \; \frac{N_{vol}}{N_{surf}} \tag{16}$$

where I_{surf} and I_{vol} is the intensity of a characteristic vibrational mode in the SERS spectrum and the normal Raman spectrum for the bulk, neat, solid sample, respectively. N_{surf} and N_{vol} are the number of molecules adsorbed on SERS active substrate and sampled in bulk, respectively illuminated under the laser spot. The analyte selected for these calculations was 4-ABT for its characteristic C-S stretching mode at 1088 cm^{-1} in Raman spectra and 1078 cm^{-1} in SERS spectra.[67] The areas were normalized to laser power and acquisition time. Three wavelengths

were employed for SEF calculation of the PEH substrates with 100, 150 and 200 nm interparticle spacing previously tested. SEF values will provide a concise assessment as to the best nano-array/wavelength combination for the studied PEH system.

The normal Raman and SERS spectrum for 4-ABT is depicted in figure 3.9 and the band assignment is illustrated in Table 3.2. There are three strong bands present among the Raman spectra of 4-ABT, the band present at 465 cm^{-1} corresponds to C-C-C bending mode while the C-C-C stretching mode is at 1592 cm^{-1}. A stretching C-S mode is present at 1088 cm^{-1} and is the band employed for the SEF calculation.

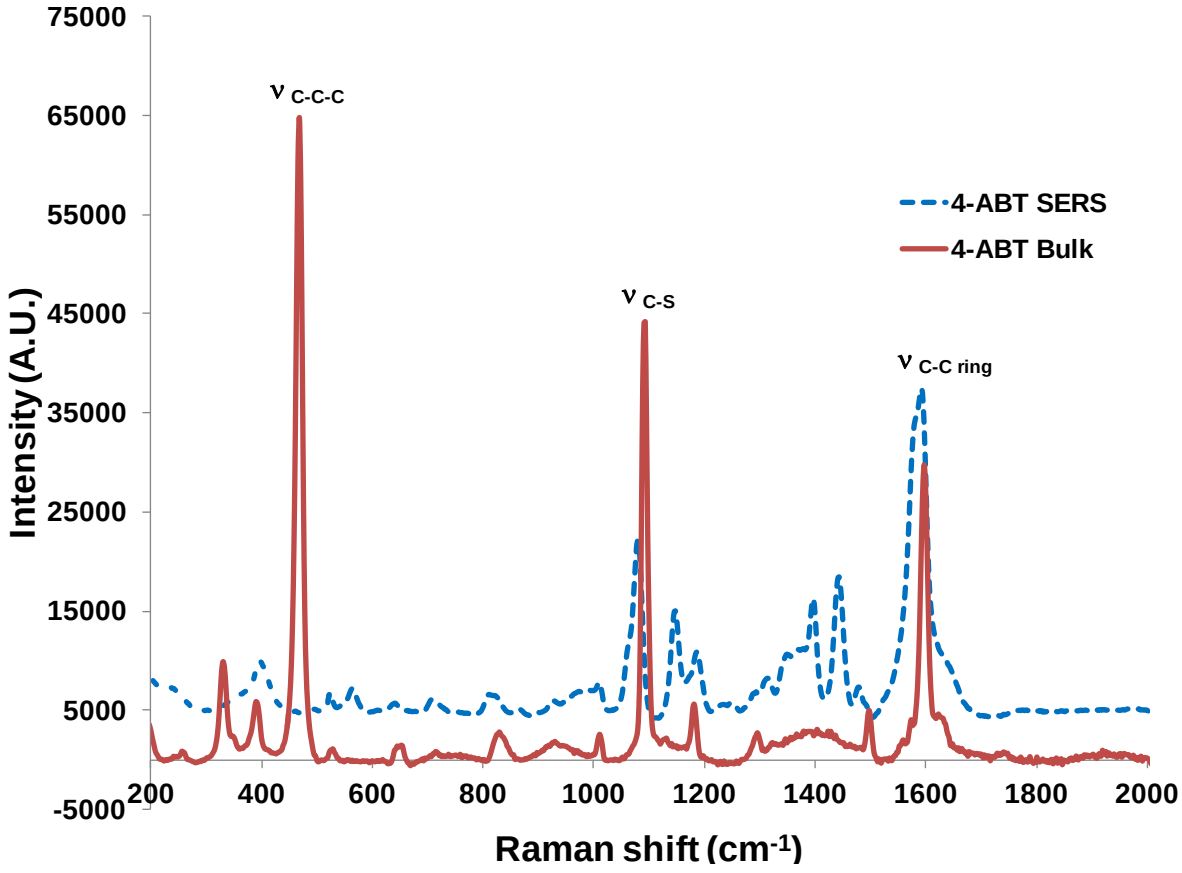

Figure 3.7. Normal Raman and SERS spectra for 4-ABT.

Table 3.2. Normal Raman and SERS band assignments for 4-aminobenzenethiol.

Assignments	4-aminobenzenethiol (cm^{-1})			
	Normal Raman		SERS	
	Lit*	Exp	Lit*	Exp
δ CH + C-S	326[a]	328		
		398		395
δ C-C-C	473[b]	465		
				493
δ C-C-C	526[a]	526	536[a]	522
				566
δ C-C-C	624[a]	639	649[a]	641
				707
ω C-H	837[a]	824	806[a]	811
δ C-C / δ C-C-C	1005[b]	1009		1011
ν C-S	1085[a]	1088	1077[a]	1078
δ C-H			1142[a]	1146
ν C-H	1176[a]	1179	1178[a]	1186
ν C-C + δ C-H		1293		
				1314
δ C-H + δ C-C			1387[a]	1395
ν C-C + δ C-H			1430[a]	1444
ν C-C + δ C-H	1492[a]	1495	1481[a]	1478
ν C-C-C	1596[a]	1592	1586[a]	1584

*** References: (a) Primera et al. [68], (b) K. Kim et al. [69]**

**** The vibrational modes were abbreviated as follows: ν: stretching, δ: bending; ω: wagging**

For 532 nm wavelength, the 50x objective with a circular laser spot, the calculated area of 1.96×10^{-7} cm^2 resulted with an integration volume of 1.77×10^{-8} cm^3. Using the density of 4-ABT, 1.18 g/cm^3, and calculated integration volume, the number of 4-ABT molecules illuminated under the laser spot area (N_{vol}) was 1.00×10^{14} molecules. Similarly, a circular laser spot is obtained with a 50x objective for the 633 nm excitation line, where the calculated laser

spot area was 9.94×10^{-7} cm^2 and the calculated integration volume was 8.95×10^{-8} cm^3. The number of 4-ABT molecules illuminated under the laser spot area (N_{vol}) was 5.08×10^{14} molecules. A 50x objective was also employed for 785 nm excitation line, whereas its rectangular-shaped laser spot area was 1.95×10^{-6} cm^2 and the calculated integration volume is 1.76×10^{-7} cm^3. The number of 4-ABT molecules illuminated under the laser spot area (N_{vol}) was 9.96×10^{14} molecules.

Estimating that 4-ABT occupies 0.19 nm^2, the packing density of 4-ABT[67,70] was calculated as $5.3x10^{14}$ molecules/cm^2. The surface area of SERS-active particles (ellipses and hexagons) under the laser spot for each nanoarray was calculated considering only the surface area of the ellipse and hexagons where the effective heights of 25 nm of Ag for each particle were also considered. Taking this into consideration, the number of molecules adsorbed on the SERS active surface (N_{surf}) (summarized in Table 3.3) was calculated multiplying effective surface area under laser spot by the 4-ABT packing density.

Table 3.3 Parameters to determine SEF

	$\lambda_{532\ nm}$ [a]			λ_{633nm} [b]			$\lambda_{785\ nm}$ [c]		
Interparticle spacing(nm)	**I_{surf} (A/mW·s)**	**N_{surf} (nm)**	**SEF**	**I_{surf} (A/mW·s)**	**N_{surf} (nm)**	**SEF**	**I_{surf} (A/mW·s)**	**N_{surf} (nm)**	**SEF**
100	$2.17x10^4$	$4.13x10^7$	$7.02x10^5$	$2.93x10^3$	$2.09x10^8$	$1.87x10^7$	$2.81x10^3$	$4.10x10^8$	$1.17x10^6$
150	$1.00x10^4$	$3.02x10^7$	$4.43x10^5$	$4.04x10^3$	$1.53x10^8$	$3.51x10^7$	$5.29x10^3$	$3.00x10^8$	$2.96x10^6$
200	$1.48x10^4$	$2.30x10^7$	$8.61x10^5$	$4.69x10^3$	$1.16x10^8$	$5.35x10^7$	$8.01x10^3$	$2.28x10^8$	$5.90x10^6$

[a] $N_{vol} = 1.00x10^{14}$ nm and $I_{vol} = 7.50x10^4$ A/mW·s

[b] $N_{vol} = 5.08x10^{14}$ nm and $I_{vol} = 3.82x10^2$ A/mW·s

[c] $N_{vol} = 9.96x10^{14}$ nm and $I_{vol} = 5.92x10^3$ A/mW·s

Surface enhancement factors calculated for PEH substrates with a 532 nm excitation line (figure 7) demonstrate that the nano-array with 200 nm interparticle spacing renders improved signal enhancement over the arrays with 100 and 150 nm interparticle spacing. As with the 532 nm, the SEF of these substrates followed an increasing trend with interparticle spacing at 633 and 785 nm. As shown in Ttable 3.3, the signal enhancement increased as function of wavelength at 532 nm, 785 nm, 633 nm with a SEF in the order of 10^5, 10^6 and 10^7, respectively. The SEF contributions include the combined contribution of the chemical and electromagnetic effect, the latter being the predominant effect. Accounting for the SEF, the best performing substrate is that of interparticle spacing of 200 nm, whereas the 633 nm wavelength is the optimum excitation line for the SERS studies of the PEH nanoarray system.

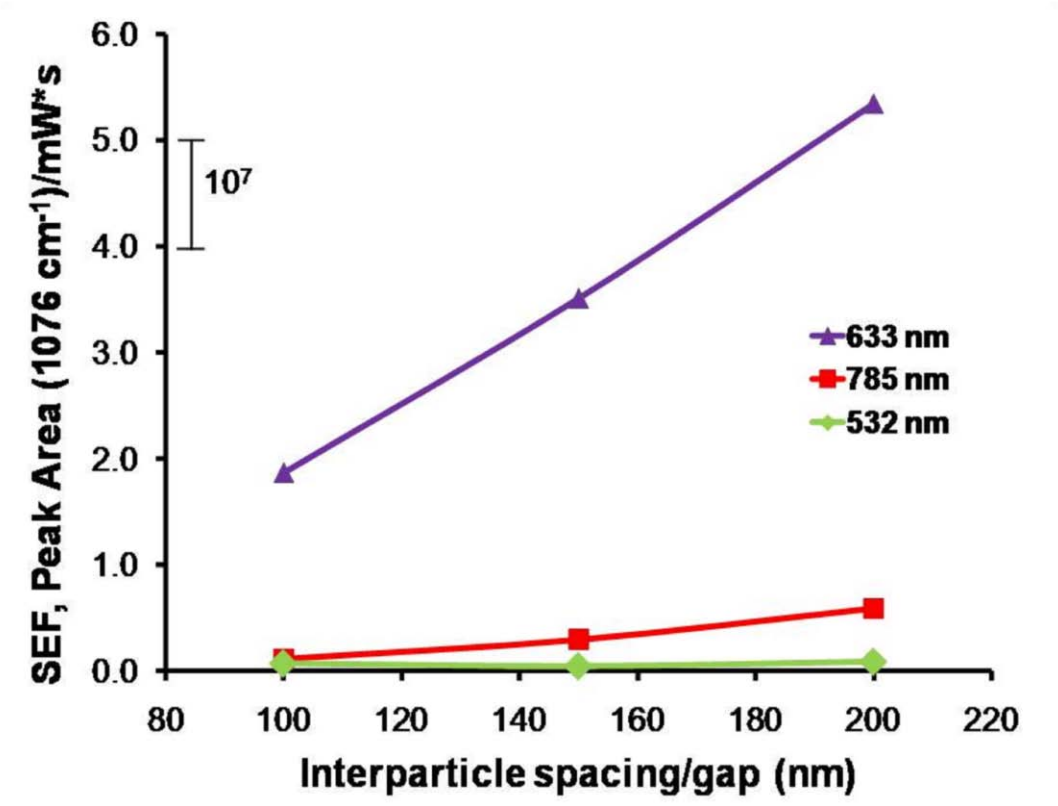

Figure 3.8. Performance of nanofabricated PEH arrays considering the 1078 cm^{-1} C-S stretching mode at 532, 633 and 785 nm.

CHAPTER 4

Concluding remarks

SERS has demonstrated to be a valuable technique for the determination and characterization of organoarsenic drugs in aqueous media. Advantages such as simple and cost effective sample preparation as well as short execution time make this technique attractive for environmental monitoring. From the spectroscopic data, we have deduced that the peaks corresponding to the arsonic group, such as symmetric stretching of As-O and As-C, can be used to identify this class of compounds. Unequivocal sample identification is obtained since each compound possesses unique spectral differences. Presence of peaks corresponding to amino, nitro and acetamido groups as well as the shifts associated with them are essential in the process of compound identification as well as assessment of orientation with respect to the silver surface. Appearance of new bands as well as shifts in the observed Raman vs. SERS signals provides structural information useful for the elucidation of interaction between the metal and the adsorbate. Surface binding of each compound has been assessed. The results indicate that 4-arsanilic acid binds to the silver surface through the amino and arsonic group. On the other hand, roxarsone and acetarsone bind through the arsonic group by formation of a monodentate complex with the silver surface.

Electron beam lithography combined with RIE has proven successful for the fabrication of nano-arrays that mimic colloidal nanoparticle aggregates, but with controlled optimization parameters such as particle morphology and orientation. Detection of 4-arsanilic acid in aqueous media was achieved employing these substrates, whereas the characteristic bands for the arsonic group as well as the amino group were present among collected SERS spectra for 633 nm

excitation line. The results demonstrate that substrates with parallel orientation (PEH) provide improved signal enhancement for 4-arsanilic acid over orthogonal orientation (OEH) and traditional Ag/PDMS nanocomposites. The effect of interparticle spacing on the SERS signal enhancement is evident where the best enhancement was obtained for substrates with 200 nm and 300 nm gap for PEH and OEH substrates, respectively. Surface enhancement factor calculations support this conclusion since the results demonstrate higher Raman enhancement for interparticle spacing of 200 nm of the PEH substrate at all three wavelengths used in the study. In addition, calculations demonstrate SERS signal enhancements for PEH substrates with maximum orders of magnitude of 10^7. The lightning rod effects mainly occur at high curvature points on the surface. The experimental conditions at which the silver films were achieved included high deposition rates resulting in a more conformal coverage, thus responses due to lightning rod effects are negligible relative to the plasmonic responses. The FDTD simulation data is consistent with the apparent SERS signal acquired for the PEH nano-arrays in which a plasmonic response is achieved at multiple excitation wavelengths (785, 633 and 532 nm, the latter being the strongest). The developed nano-arrays result in an attractive alternative for the detection and study of arsenic drugs in aqueous media at trace levels.

Future studies could be focused at the fabrication of hybrid nano-arrays with larger surface areas which could lead to a substrate with improved quantification capabilities. Another fabrication parameter that could be explored is the orientation of the hexagon relative to the ellipse, whereas the vertices of the hexagon would be parallel to the ellipse. This consideration could provide an improved propagation of the surface plasmons on the nanoparticle surface and therefore result in increased signal enhancements.

An area that could be further explored is the use of Ag/PDMS and hybrid nano-arrays for biosensing. Preliminary experiments demonstrate the ability of Ag/PDMS substrates to detect bacteria such as *Bacillus thuringiensis* (Bt) and E.Coli. Additional experimentation is required to determine the viability of these substrates as sensors not only for the detection of bacteria but of the discrimination of these organisms.

REFERENCES

1. Kneipp, K.; Kneipp, H.; Itzkan, I.; Dasari, R. R.; Feld, M. S. Surface-enhanced Raman scattering and biophysics. *J. Phys. Condens. Matter*. **2002**, *14(18)*, pp 597-524.

2. Le Ru, E.C.; Etchegoin, P.G. Principles of surface-enhanced Raman spectroscopy and related plasmonic effects. 1st Ed.; Elsevier, 2009.

3. McCreery, R. Raman spectroscopy for chemical analysis. Wiley-Interscience, Vol. 157, 2000.

4. Ferraro, J.R.; Nakamoto, K.; Brown, C.W. Introductory Raman Spectroscopy. 2nd Ed.; Elsevier, 2003.

5. Vo-Dihn, T. Surface-enhanced Raman spectroscopy using metallic nanostructures. *Trends Anal. Chem.* **1998**, *17(nos. 8+9)*, pp 557-581.

6. Fleischmann, M.; Hendra, P. J.; McQuillan, A. J. Raman spectra of pyridine adsorbed at a silver electrode. *Chem. Phys. Lett.* **1974**, *26*, pp 163-166.

7. Kosuda, K. M.; Bingham, J. M.; Wustholz, K. L.; Van Duyne, R. P. Nanostructures and surface-enhanced Raman spectroscopy. In *Andrews, D.L.; Scholes, G.D.; Wiederrecht, G.P. (eds.) Comprehensive Nanoscience and Technology*, Oxford Academic Press: 2011; Vol. 3, pp 263-301.

8. Campion, A.; Kambhampati, P. Surface-enhanced Raman Scattering. *Chem. Soc. Rev.* **1998**, *27*, pp 241-250.

9. Schlücker, S. Ed. Surface enhanced Raman spectroscopy. Analytical, biophysical and life science applications; Wiley-Vch: Weinheim, Germany, 2011.

10. Kneipp, K.; Kneipp, H.; Itzkan, I.; Dasari, R. R.; Feld, M. S. Surface-enhanced Raman scattering and biophysics. *J. Phys. Condens. Matter*. **2002**. *14(18)*, pp 597-524.

11. Raj, A.; Raju, K.; Varghese, H. T.; Granadeiro, C. M.; Nogueira, H. I. S.; Yohannan Panicker C. IR, Raman and SERS spcectra of 2-(methoxycarbonylmethylsulfanyl)-3,5-dinitrobenzene carboxyl acid. *J. Braz. Chem. Soc.* **2009**, *20(3)*, pp 549-559.

12. Fleger, Y.; Mastai, Y.; Rosenbluh, M.; Dressler, D. H. Surface-enhanced Raman spectroscopy as probe for adsorbate orientation on silver nanoclusters. *J. Raman Spectrosc.* **2009**, *40(11)*, pp 1572-1577.

13. Le Ru, E. C.; Blackie, M. M.; Meyer, M.; Etchegoin, P. G. Surface Enhanced Raman Scattering Enhancement Factors: A Comprehensive Study. *J. Phys. Chem. C.* **2007**, *111*, pp 13794-13803.

14. Jeanmaire, D. L.; Van Duyne. R. P. Part I. Heterocyclic, aromatic, and aliphatic amines adsorbed on the anodized silver electrode. *J. Electroanal. Chem.* **1977**, *84(1)*, pp 1-20.

15. Albrecht, M. G.; Creighton, J.A. Anomalously intense Raman spectra of pyridine at a silver electrode. *J. Am. Chem. Soc.* **1977**, *99*, pp 5215-5217.

16. Vo-Dinh, T.; Dhawn, A.; Norton, S. J.; Khoury, C. G.; Wang, H-N.; Misra, V.; Gerhold, M.D. Plasmonic nanoparticles and nanowires: design, fabrication and application in sensing. *J. Phys. Chem. C.* **2010**, *114(16)*, pp 7480-7488.

17. Rommanato, F.; Pilot, R.; Massari, M.; Ongarello, T.; Pirruccio, G.; Zilio, P.; Ruffato, G.; Carli, M.; Sammito, D.; Giorgis, V.; Garoli, D.; Signorini, R.; Schiavuta, P.; Bozio; R. Design, fabrication and characterization of plasmonic gratings for SERS. *Microelectron. Eng.* **2011**, *88*, pp 2717-2720.

18. Yokota, Y.; Ueno, K.; Juodkazis, S.; Mizeikis, V.; Murazawa, N.; Misawa, H.; Kasa, H.; Kintaka, K.; Nishii. J. Nano-textured metallic surfaces for optical sensing and detection applications. *J. Photochem. Photobiol. A.* **2009**, *207 (1),* pp 126-134.

19. Fan, M.; Andrade, G. F. S.; Brolo, A. G. A review on the fabrication of substrates for surface enhanced Raman spectroscopy and their applications in analytical chemistry. *Anal. Chim. Acta*. **2011**, *693*, pp 7-25.

20. Mattox, D.M. Physical vapor deposition (PVD) process. *Met. Finish.* **2001**, *99*, pp 409-423.

21. Olavarría-Fullerton, J.; Wells, S.; Ortiz-Rivera, W.; Sepaniak, M. J.; De Jesús, M. A. Surface-Enhanced Raman Scattering (SERS) Characterization of Trace Organoarsenic Antimicrobials Using Silver /Polydimethylsiloxane Nanocomposites. *Appl. Spectrosc.* **2011**, *65*, pp 423-428.

22. Ventra, M. Di.; Evoy, S.; Heflin Jr., J.R. Ed. Introduction to nanoscale science and technology. Intro nanoscale, Springer, 2004.

23. Bhushan, B. Handbook of Nanotechnology. Springer, 2004.

24. Das, G.; Mercarini, F.; Gentile, F.; De Angelis, F.; Kumar, HG. M.; Candelero, P.; Liberale, C.; Cuda, G.; Di Fabrizio, E. Nano-patterned SERS substrate: Application for protein analysis vs. temperature. *Biosens. Bioelectron.* **2009**, *24 (6),* pp 1693-1699.

25. Kahl, M.; Voges, E.; Kostrewa, S.; Viets, C; Hill, W. Periodically structured metallic substrates for SERS. *Sens. Actuators, B.* **1998**, *51*, pp 285-291.

26. Abu Hatab, N. A.; Oran, J. M.; Sepaniak, M.J. Nanotransfer printing (nTP) for surface enhanced Raman spectroscopy (SERS). *ACS Nano*. **2008**, *2(2),* pp 377-385.

27. Barcelo, S.J.; Kim, A.; Wu, W.; Li, Z. Fabrication of deterministic nanostructure assemblies with sub-nanometer spacing using nanoimprinting transfer. *ACS Nano*. **2012**, *6(7),* pp 6446-6452.

28. Wells, S.; Retterer, S. D.; Oran, J. M.; Sepaniak, M. J. Controllable nanofabrication of aggregate-like nanoparticle substrates and evaluation for surface enhanced Raman spectroscopy. *ACS Nano.* **2009**, *3*, pp 3845-3853.

29. De Jesús, M. A.; Giesfeldt, K.S.; Oran, J.M.; Abu-Hatab, N.A.; Lavrik, N.V.; Sepaniak, M.J. Nanofabrication of densely packed polymer-metal arrays for surface enhanced Raman spectrometry. *Appl. Spectrosc.* **2005**, *59(12),* pp 1501-1508.

30. Oran, J. M.; Hinde, R. J.; Hatab, N. A.; Retterer, S. T.; Sepaniak, M.J. Nanofabricated periodic arrays of silver elliptical discs as SERS substrates. *J. Raman Spectrosc.* **2008**, *39*, pp 1811-1820.

31. Chapman, H.; Johnson, Z. Use of antibiotics and roxarsone in broiler chickens in the USA: analysis for the years 1995 to 2000. *Poult Sci.* **2002,** *81(3),* pp 356-364.

32. Morrison, J. L. Distribution of arsenic from poultry litter in broiler chickens, soli and crops. *J. Agric. Food. Chem*. **1969**, *17(6),* pp 1288-1290.

33. http://usda.mannlib.cornell.edu/usda/current/PoulProdVa/PoulProdVa-04-29-2010.pdf, USDA, "Poultry Production and Value", (2009).

34. Jackson, B. P.; Bertsch, P. M; Cabrera, M. L.; Camberato, J. J.; Seaman, J.C.; Wood, C.W. Trace element speciation in poultry litter. *J. Environ. Qual.* **2003**, *32*, pp 535-540.

35. Garbarino, J. R.; Bednar, A. J.; Rutherford, D. W.; Beyer, R. S.; Wershaw, R. L. The environmental fate of roxarsone in poultry litter: Part I, Degradation of roxarsone during composting. . *Environ. Sci. Tech.* **2003**, *37(8),* pp 1509-1514.

36. Stolz, J. F.; Perera, E.; Kilonzo, B.; Kail, B.; Crable, B.; Fisher, E.; Ranganathan, M.; Wormer, L.; Basu, P. Biotransformation of 3-nitro-4-hydroxybenzene arsonic acid and release of inorganic arsenic by *Clostridium* species. *Environ. Sci. Tech.* **2007**, *41*, pp 818-823.
37. Cortinas, I.; Field, J. A.; Kopplin, M.; Garbarino, J. R.; Gandolfi, A. J.; Sierra-Alvarez, R. Anaerobic biotransformation of roxarsone and related N-substituted phenylarsonic acids. . *Environ. Sci. Tech.* **2006**, *40(9)*, pp 2951-2957.
38. Rosal, C. G.; Momplaisir, G.-M.; Heithmar, E. M. Roxarsone and transformation products in chicken manure: determination by capillar electrophoresis-inductively coupled plasma-mass spectrometry. *Electrophoresis*. **2005**, *26(7-8)*, pp 1606-1614.
39. Jackson, B. P.; Bertsch, P. M. Determination of arsenic speciation in poultry wastes by IC-ICP-MS. *Environ. Sci. Tech.* **2001**, *35(24)*, pp 4868-4873.
40. Roerdink, A. R.; Aldstadt, J. H. Sensitive method for the determination of roxarsone using solid-phase microextraction with multidetector gas chromatography. *J. Chromatogr. A* **2004**, *1057(1-2)*, pp 177-183.
41. Kneipp, K. Raman spectroscopy of single molecules. *Single Mol*. **2001**, *2*, *pp* 291-292.
42. Futamata, M. Single molecule sensitivity in surface enhanced Raman scattering. Proceedings of SPIE-The International Society for Optical Engineering, *Plasmonic Nano-Imaging Nanofabr.* **2005**, *5928*.
43. Rivas, L.; Sánchez-Cortés, S.; García-Ramos, J. V.; Morcillo, G. Growth of Silver Colloidal Particles Obtained by Citrate Reduction to Increase the Raman Enhancement Factor *Langmuir*. **2001**, *17*, pp 574-577.

44. Lee, Y.-H.; Dai, S.; Young, J. P. Silver-doped sol-gel films as the substrate for surface-enhanced Raman scattering. *J. of Raman Spectrosc.* **1997**, *28(8)*, pp 635-639.

45. De Jesús, M. A.; Giesfeldt, K. S.; Sepaniak , M. J. Improving the figures of merit of SERS in the analysis of model environmental pollutants. *J. of Raman Spectrosc.* **2004**, *35 (10)*, pp 895-904.

46. Giesfeldt, K. S.; Connatser, R. M.; De Jesus, M. A.; Lavrik, N. V.; Dutta, P. S.; Sepaniak, M. J. Studies of the optical properties of metal-pliable polymer composite materials. *Appl. Spectrosc.* **2003**. 57(11), pp 1346-1352.

47. Melamed, D. Monitoring arsenic in the environment: a review of science and technologies with the potential for field measurements. *Anal. Chim. Acta* **2005**, *532(1)*, pp 1-15.

48. Raj, A.; Raju, K.; Varghese, H. T.; Granadeiro, C. M.; Nogueira, H. I. S.; Yohannan Panicker, C. IR, Raman and SERS spcectra of 2-(methoxycarbonylmethylsulfanyl)-3,5-dinitrobenzene carboxyl acid. *J. Braz. Chem. Soc.* **2009**, *20(3)*, pp 549-559.

49. Fleger, Y.; Mastai, Y.; Rosenbluh, M.; Dressler, D. H. Surface-enhanced Raman spectroscopy as probe for adsorbate orientation on silver nanoclusters. *J. of Raman Spectrosc.* **2009**, *40(11)*, pp 1572-1577.

50. Baltussen, E.; Cramers, C.; Sandra, P. Sorptive sample preparation- a review. *Analytical and Bioanalytical Chemistry* **2002**, *373(1)*, pp 3-22.

51. Baltussen, E.; David, F.; Sandra, P.; Janssen, H.-G.; Cramers, C. Equilibrium sorptive enrichment on poly(dimethylsiloxane) particles for trace analysis of volatile compounds in gaseous samples. *Anal. Chem*. **1999**, *71(22)*, pp 5193-5198.

52. Cowen, S.; Duggal, M.; Hoang, T.; Al-Abadleh, H. A. Vibrational spectroscopic characterization of some environmentally impostant organoarsenicals A guide for

understanding the nature of their surface complexes. *Can. J. Chem.* **2008**, *86(10)*, pp 942-950.

53. Haresh, R.; Philip, D.; Aruldhas, G. Infrared, Raman, and SERS spectra of betaine arsenate. Spectrosc. Lett. **1995**, *28(1)*, pp 11-28.
54. Aroca, R. *Surface-Enhanced Vibrational Spectroscopy* (John Wiley & Sons, 2006).
55. Myneni, S. C. B.; Traina, S. J.; Waychunas, G. A.; Logan, T. J. Experimental and theoretical vibrational spectroscopic evaluation of arsenate coordination in aqueous solutions, and at mineral-water interfaces. *Geochim. et Cosmochim. Acta* **1998**, *62(19-20)*, pp 3285-3300.
56. Suh, J. S.; Kim, J. Three distinct geometries of surface-adsorbed carboxylate groups. *J. Raman Spectrosc.* **1998**, *29(2)*, pp 143-148.
57. Smith, M.; Stambaugh, K.; Smith, L.; Son, H.-J.; Gardner, A.; Cordova, S.; Posey, K.; Perry, D.; Biris, A. S. Surface-enhanced vibrational investigation of adsorbed analgesics. *Vib. Spectrosc.* **2009**, *49(2)*, pp 288-297.
58. Wang, Y.; Li, Y.-S.; Zhang, Z.; An, D. Surface-enhanced Raman scattering of some water insoluble drugs in silver hydrosols. *Spectrochim. Acta Mol.* **2003**, *59 (3)*, pp 589-594.
59. Cañamares, M.V.; García-Ramos, J.V.; Sanchez-Cortes, S.; Castillejo, M.; Oujja, M. Comparative SERS effectiveness of silver nanoparticles prepared by different methods: A study of the enhancement factor and interfacial properties. *J. Colloid Interface Sci.* **2008**, *326 (1)*, pp 103-109.
60. Camden, J.P.; Dieringer, J.A.; Zhao, J.; Van Duyne, R.P. Controlled Plasmonic Nanostructures for Surface-Enhanced Spectroscopy and Sensing. *Acc. Chem. Res.* **2008**, *41(12)*, pp 1653-1661.

61. Barcelo, S.J.; Kim, A.; Wu, W.; Li, Z. Fabrication of Deterministic Nanostructure Assemblies with Sub-nanometer Spacing using a Nanoimprinting Transfer Technique. *ACS Nano.* **2012**, *6 (7),* pp 6446-6452.

62. Petryayeva, E.; Krull, U. J. Localized surface plasmon resonance: Nanostructures, bioassays and biosensing- A review. *Anal. Chim. Acta.* **2011**, *706(1),* pp 8-24.

63. Forestiere, C. ; Giovanni, G.; Boriskina, S.V.; Negro, L.D. The role of nanoparticle shapes and deterministic aperiodicity for the design of nanoplasmonic arrays. *Opt. Express*. **2009**, *17(12),* pp 9648-9661.

64. *ZEP520A: High Resolution Positive Electron Beam Resist*; Technical Report No. ZEP520 Version 1.02 for ZEONREX Electric Chemicals: Japan, March 2001.

65. Lumerical Solutions, Inc. *FDTD Solutions Knowledge Base Version 7.5*. http://www.lumerical.com/support/knowledge_base.html (accessed June 2012).

66. Bijeon, J.L.; Royer, P.; Goudonnet, J.P.; Warmack, R.J.; Ferrell, T.L. "Effects of a Silicon Substrate on Surface Plasmon Spectra in Silver Island Films". *Thin Solid Films*. **1987**, *155(1),* pp L1-L3.

67. Yong, S.Y.; Hung, L.; Lang, G.S.; Cornett, J.E.; Mayergoyz, I.D.; Rabin, O. Dispersion in the SERS Enhancement with Silver Nanocube Dimers. *ACS Nano*. **2010**, *4(10),* pp 5763-5772.

68. Primera-Pedrozo, O.P. Synthesis and surface modification of metallic nanoparticles: sensitivity, influence of shape, concentration and excitation wavelength on chemical detection by SERS. PhD thesis, University of Puerto Rico, Mayaguez Campus, P.R., **2010**.

69. Kim, K.; Shin, D.; Choi, J-Y.; Lock Kim, K.; Soo Shin, K. Surface-enhanced Raman scattering characteristics of 4-aminobenzenethiol derivatives adsorbed on silver. *J. Phys. Chem. C.* **2011**, *115*, pp 24960-24966.

70. Gole, A.; Sainkar, S.R.; Sastry, M. Electrostatically Controlled Organization of Carboxylic Acid Derivatized Colloidal Silver Particles on Amine-Terminated Self-Assembled Monolayers. *Chem. Mater.* **2000**, *12(5)*, pp 1234-1239.

APPENDIX

Surface enhancement factor: the detailed calculation

For 532 nm wavelength, the 50x objective with a circular laser spot with a diameter of 5 μm or 0.0005 cm. The laser spot area in cm^2 is:

$$Laser\ spot\ area = \frac{\pi d^2}{4}$$

$$Laser\ spot\ area = \frac{\pi(0.0005\ cm)^2}{4} = 1.96 \times 10^{-7}\ cm^2$$

where the integration volume can be calculated with the 0.09 cm penetration volume,

$$Integration\ volume = \ laser\ spot\ area\ \times height$$

$$Integration\ volume = \ 1.96 \times 10^{-7} cm^2\ \times 0.09\ cm = 1.77 \times 10^{-8}\ cm^3$$

As previously mentioned, the probe molecule selected for SEF calculations was 4-ABT, since it is has been widely studied where has the capacity to form a monolayer over the nanostructured silver surface with a specific orientation. This molecule occupies ~0.19 nm[89, 90] over the silver surface.

Using the density of solid 4-ABT, 1.18 g/cm^3, and calculated integration volume, the number of 4-ABT molecules illuminated under the laser spot area (N_{vol}) is,

$$N_{vol} = 1.18\ \frac{g}{cm^3} \times 1.8x10^{-8}\ cm^3\ \times \frac{1\ mol\ 4ABT}{125.19\ g} \times \frac{6.023x10^{23}\ molecules}{1\ mol\ 4ABT}$$

$$N_{vol} = 1.00 \times 10^{14}\ molecules\ 4ABT$$

Since 4-ABT is estimated to occupy 0.19 nm^2 then,

$$\frac{1\ molecule}{0.19\ nm^2} \times \frac{(1.0x10^9\ nm)^2}{1\ m^2} \times \frac{1\ m^2}{(100\ cm)^2} = 5.26\ x10^{14}\ \ molecule/cm^2$$

To determine the N_{surf}, the effective surface area of the nanostructures under the laser spot must be determined. The effective surface area is considered area that contributes to SERS enhancement, in this case, the superior area of the nanostructure and the lateral area of the nanostructure that is composed of Ag (25 nm in height). For example, the effective surface area of an array of 100 nm of interparticle spacing determined as follows:

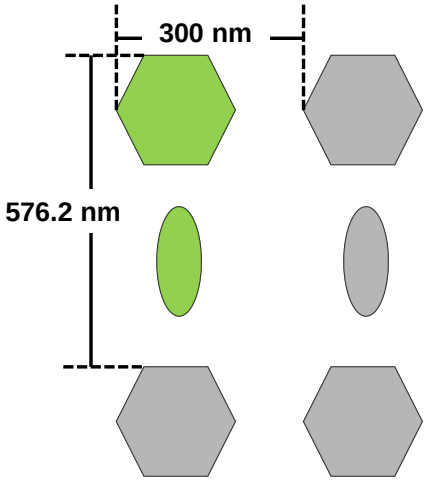

Figure A.1. Schematic illustration of the nanostructures within a PEH nanoarray of 100 nm interparticle spacing.

For this calculation, a unit was defined as the area that contains one ellipse and one hexagon. For example, a unit for a PEH array is the area of 300 nm x 576.2 nm that contains one ellipse and one hexagon (illustrated in figure 3.7, where green features represents the ellipse/hexagon within the unit).

The unit area is then defined as,

$$Area\ of\ the\ unit = lenght\ \times width$$

$$Area\ of\ the\ unit = 576.2\ nm\ \times 300\ nm = 172860\ nm^2 = 1.72860\ cm^2$$

The surface area of SERS-active particles (ellipses and hexagons) under the laser spot for each nanoarray was calculated considering only the surface area of the ellipse and hexagons, where the effective heights of 25 nm of Ag for each particle were also considered. One ellipse and one hexagon and their respective lateral areas is composed within the unit area. The area of an ellipse with its lateral area is determined as follows:

$$Area\ of\ an\ ellipse = 2L\pi\sqrt{\tfrac{1}{2}(a^2 + b^2)} + \pi ab$$

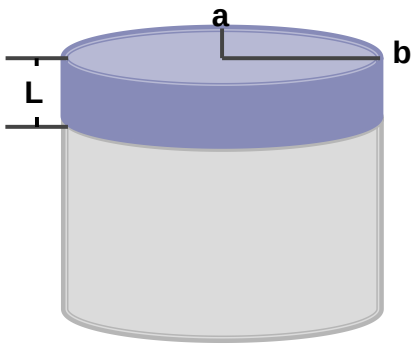

Figure A.2. Illustration of an ellipse nanostructure.

$$Area\ of\ an\ ellipse = 2(25\ nm)\pi\sqrt{\tfrac{1}{2}((100\ nm)^2 + (50\ nm)^2)} + 2\pi(50\ nm)(100\ nm)$$

$$Area\ of\ an\ ellipse = 12418.24\ nm^2 + 15707.96\ nm^2 = \ 28126.2\ nm^2$$

The area and lateral area of a hexagon is determined as,

$$Area\ of\ a\ hexagon = \frac{3\sqrt{3}\,L^2}{2}$$

$$Area\ of\ a\ hexagon = \frac{3\sqrt{3}\,(100\ nm)^2}{2} = 25980.76\ nm^2$$

$$Lateral\ area\ of\ hexagon = perimeter\ \times height$$

$$Area\ of\ height = 600\ nm\ \times 25\ nm = 15000\ nm^2$$

Therefore, the area of an ellipse and a hexagon within a unit is:

$$Area\ of\ hexagon\ and\ an\ ellipse = 25980.76\ nm^2 + 15707.96\ nm^2 = 41688.72\ nm^2$$

$$41688.72\ nm^2 = 4.168872 \times 10^{-10}\ cm^2$$

The lateral area of an ellipse and a hexagon within a unit is:

$$Lateral\ area\ of\ hexagon\ and\ an\ ellipse = 15000\ nm^2 + 12418.24\ nm^2 = 27418.24\ nm^2$$

$$27418.24\ nm^2 = 2.74182 \times 10^{-10}\ cm^2$$

Based on the effective areas within the unit, the effective surface area for the PEH nanoarray with 100 nm unterparticle spacing can be calculated as;

$$Surface\ area\ under\ laser\ spot = \frac{Spot\ area}{Unit\ size} \times (effective\ surface\ area)$$

$$Surface\ area\ under\ laser\ spot$$

$$= \frac{(1.95 \times 10^{-7}\ cm^2)}{(1.7286 \times 10^{-9} cm^2)} \times (4.16887 \times 10^{-10} cm^2 + 2.74182 \times 10^{-10} cm^2)$$

$$Surface\ area\ under\ laser\ spot = 7.85 \times 10^{-8} cm^2$$

The surface area under the laser spot was determined for each array with different interparticle spacings . Taking into account the effective surface area under the laser spot and assuming a full monolayer of 4-ABT, N_{surf} for a PEH substrate with 100 nm interparticle spacing is calculated as,

$$N_{surf} = 5.26 \times 10^{14} \frac{molecules}{cm^2} \times 7.85 \times 10^{-8} cm^2 = 4.13 \times 10^{7}\ molecules$$

As noted the C-S vibrational mode is shifted within SERS spectra to 1078 cm^{-1} indicating the formation of a complex with the silver surface. Since the intensity of the C-S band at 1088 cm^{-1} in the normal Raman spectra is 75010.72 area·mW^{-1}·s^{-1} and its intensity in SERS spectra (1078 cm^{-1}) is 32234.23 area·mW^{-1}·s^{-1}, the SEF value can be calculated as:

$$SEF = \frac{I_{surf}}{I_{bulk}}\ X \frac{N_{bulk}}{N_{surf}}$$

$$SEF = \frac{322234.23\ \frac{Area}{mW \cdot s}}{75010.72\ \frac{Area}{mW \cdot s}}\ X \frac{1.00 \times 10^{14}\ \frac{Area}{mW \cdot s}}{41314602.04\ \frac{Area}{mW \cdot s}}$$

$$SEF = 1.04 \times 10^{6}$$

All SEF values for 4-ABT employing PEH nanostructures were determined in the same manner as the previous example. The values for N_{vol}, I_{vol}, I_{surf}, N_{surf} and SEF for this excitation line are summarized in table 3.3.

A 50x objective was also employed for 785 nm excitation line, however the laser spot is rectangular-shaped with a length of 0.0015 cm and 0.0013 cm. The laser spot area can be determined as,

$$Laser\ spot\ area = \ Lenght\ X\ width$$

$$Laser\ spot\ area = \ 0.0015\ cm\ \times 0.0013\ cm$$

$$Laser\ spot\ area = \ 1.95 \times 10^{-6}\ cm^2$$

where the integration volume can be determined considering the penetration volume of 0.09 cm,

$$Integration\ volume = \ laser\ spot\ area\ \times height$$

$$Integration\ volume = \ 1.95 \times 10^{-6} cm^2\ \times 0.09\ cm = 1.76 \times 10^{-7}\ cm^3$$

Similarly, the number of 4-ABT molecules illuminated under the laser spot area for 785 nm excitation wavelenghht (N_{vol}) employing the calculated integration volume was,

$$N_{vol} = 1.18\ \frac{g}{cm^3} \times 1.76x10^{-7}\ cm^3\ \times \frac{1\ mol\ 4ABT}{125.19\ g} \times \frac{6.023x10^{23}\ molecules}{1\ mol\ 4ABT}$$

$$N_{vol} = 9.96 \times 10^{14}\ molecules\ 4ABT$$

Estimating that 4-ABT occupies 0.19 nm^2, the packing density of 4-ABT[24,25] was calculated as $5.3x10^{14}$ molecules/cm^2. Similarly to the previous example, the effective surface area of the nanostructures must be determined. The area of the ellipse and hexagons and their lateral areas within the unit is the same values at the different interparticle spacings however since the laser spot is not the same the value of the N_{surf} varies from the values obtained for the 532 nm excitation wavelength. The number of molecules adsorbed on the SERS active surface (N_{surf}) employing 785 nm excitation wavelength is summarized in Table 3.3.